Colloquium: Inclusions, boundaries, and disorder in scalar active matter

Omer Granek and Yariv Kafri

Department of Physics, Technion—Israel Institute of Technology, Haifa 32000, Israel

Mehran Kardar, Sunghan Ro, and Julien Tailleur

Department of Physics, Massachusetts Institute of Technology, Cambridge, Massachusetts 02139, USA

Alexandre Solon

Sorbonne Université, CNRS, Laboratoire de Physique Théorique de la Matière Condensée (UMR CNRS 7600), 4 Place Jussieu, 75252 Paris Cedex 05, France

(published 30 September 2024)

Active systems are driven out of equilibrium by exchanging energy and momentum with their environment. This endows them with anomalous mechanical properties that are reviewed in this Colloquium. The case of dry scalar active matter is considered, which encompasses systems whose large-scale behaviors are entirely captured by their density—a scalar field. Arguably the simplest of active-matter systems, they have attracted considerable attention due to their unusual properties when put in contact with boundaries, inclusions, tracers, or disordered potentials. Indeed, studies of the mechanical pressure of active fluids and of the dynamics of passive tracers have shown that active systems impact their environment in nontrivial ways, for example, by propelling and rotating anisotropic inclusions. Conversely, the long-range density and current modulations induced by localized obstacles show how the environment can have a far-reaching impact on active fluids. This is best exemplified by the propensity of bulk and boundary disorder to destroy bulk phase separation in active matter, thereby showing active systems to be much more sensitive to their surroundings than passive ones. This Colloquium aims to provide a unifying perspective on the rich interplay between active systems and their environments.

DOI: 10.1103/RevModPhys.96.031003

CONTENTS

I. INTRODUCTION

Active matter comprises entities that dissipate energy to exert propelling forces on their environment (Ramaswamy, 2010; Marchetti *et al.*, 2013; Bechinger *et al.*, 2016; Fodor and Marchetti, 2018; Chaté, 2020; Tailleur *et al.*, 2022). From molecular motors to bacteria and large groups of animals, active systems are ubiquitous in biology. Furthermore, over the past two decades, physicists and chemists have devised active particles in the lab, paving the way toward engineering synthetic active materials using Janus colloids (Paxton *et al.*, 2004; Howse *et al.*, 2007; Palacci *et al.*, 2010, 2013; Nishiguchi and Sano, 2015; Yan *et al.*, 2016), vibrated grains (Narayan, Ramaswamy, and Menon, 2007; Deseigne,

Dauchot, and Chaté, 2010), Quincke rollers (Bricard *et al.*, 2013; Liu *et al.*, 2021), or self-propelled droplets (Herminghaus *et al.*, 2014; Izzet *et al.*, 2020). The nonequilibrium drive at the microscopic scale endows active materials with a plethora of collective behaviors that are unmatched in equilibrium physics. The rich contrast with equilibrium has germinated considerable experimental and theoretical research on the subject, which has turned active matter into a central field of condensed matter physics.

One of the most striking differences between active and passive systems lies in their manifestations of force and work, which runs counter to intuition from equilibrium thermodynamics. While in some aspects bulk fluids of active particles resemble equilibrium matter, the forces exerted on their confining vessels (Takatori, Yan, and Brady, 2014; Yang, Manning, and Marchetti, 2014; Solon, Fily *et al.*, 2015; Junot *et al.*, 2017; Zakine *et al.*, 2020) display a host of unusual phenomena. Examples range from ratchet currents (Di Leonardo *et al.*, 2010; Sokolov *et al.*, 2010; Reichhardt and Reichhardt, 2017) to anisotropic pressure (Solon, Fily *et al.*, 2015) and long-range density modulations induced by inclusions (Galajda *et al.*, 2007; Tailleur and Cates, 2009; Angelani, Costanzo, and Di Leonardo, 2011; Baek *et al.*, 2018; Rodenburg *et al.*, 2018). More recently it became clear that the set of results pertaining to boundaries, inclusions, and tracers, and to the forces exerted on them, have a much broader impact in the context of disordered active materials (Morin *et al.*, 2017; Toner, Guttenberg, and Tu, 2018a; Chardac *et al.*, 2021; Duan *et al.*, 2021). In particular, disorder has been shown to play a fundamentally different role for active systems than for equilibrium ones (Ben Dor *et al.*, 2019; Ro *et al.*, 2021; Ben Dor, Ro *et al.*, 2022).

In this Colloquium, we review recent results on scalar active matter in the presence of boundaries, inclusions, tracers, and disorder, for which we try to offer a coherent physical picture. Scalar systems correspond to "dry" active matter whose only hydrodynamic mode is the conserved density field. It offers the simplest-yet-not-too-simple framework to study the interplay between activity and mechanical forces. The insights gained from studying these systems can then be used in other situations, such as "wet" active matter, where the presence of a momentum-conserving solvent plays an important role. Similarly, the interplay between activity and mechanics in polar or nematic active fluids forms a current frontier of the field that is beyond the scope of this Colloquium.

We first introduce scalar active matter in Sec. II, starting at the single-particle level and progressing to collective behaviors. In Sec. III, we discuss the anomalous properties of the forces that active fluids exert on confining boundaries. In Sec. IV, we turn to obstacles and tracers immersed in active baths. The results presented in these sections finally allow us to discuss the effect of bulk and boundary disorder on active fluids in Secs. V and VI, respectively.

II. SCALAR ACTIVE MATTER

To introduce scalar active matter at the microscopic scale, we first review the standard models of active particles in Sec. II.A. We then discuss in Sec. II.B the different interactions between particles that have been considered, and the conditions under which the resulting large-scale physics reduces to a dynamics that can be written solely in terms of a density field. Finally, we describe the collective behaviors encountered in scalar active systems in Sec. II.C, focusing on motility-induced phase separation (MIPS), and we review the corresponding hydrodynamic description in Appendix A.1.

A. Noninteracting active particles

A large diversity of active particles, each capable of dissipating energy to self-propel, exists across scales in nature, from molecular motors at the nanoscale to cells and macroscopic animals. In addition, many types of artificial self-propelled particles are now engineered, with examples including chemically powered Janus colloids (Howse *et al.*, 2007), colloidal rollers (Bricard *et al.*, 2013), vibrated grains (Deseigne, Dauchot, and Chaté, 2010), self-propelled droplets (Thutupalli, Seemann, and Herminghaus, 2011), and "hexbug" toy robots (Li and Zhang, 2013). Although they vary greatly in their details, these active particles share the feature of being persistent random walkers. Compared to a passive random walker, this introduces a typical scale separating ballistic motion at a small scale from a diffusive behavior on large scales. This scale is quantified by the persistence time τ and the average distance traveled during this time, which is called the persistence length ℓ_p. Three types of active particles have been most commonly used in theoretical and numerical studies of active matter: active Brownian particles (ABPs) (Fily and Marchetti, 2012), run-and-tumble particles (RTPs) (Schnitzer, 1993), and active Ornstein-Uhlenbeck particles (AOUPs) (Hänggi and Jung, 1994; Sepúlveda *et al.*, 2013; Szamel, 2014).

ABPs and RTPs propel at a constant speed $v_p = \mu f_p$, where μ is the particle mobility and f_p is the constant magnitude of the self-propelling force. The orientations of ABPs change continuously due to rotational diffusion, characterized by a rotational diffusivity D_r. By contrast, RTPs randomize their directions of motion instantaneously during "tumbles" that occur at a constant rate α. ABPs are a good model for self-propelled colloids (Howse *et al.*, 2007; Ginot *et al.*, 2018), while RTPs have been used to model the dynamics of swimming bacteria like *E. coli* (Berg, 2004). The spatial dynamics of RTPs and ABPs, in their simplest form, read

$$\dot{\mathbf{r}}(t) = \mu \mathbf{f}_p(t), \tag{1}$$

where the self-propulsion force $\mathbf{f}_p(t)$ can be seen as a non-Gaussian noise of fixed magnitude f_p. The persistence time of an ABP in d space dimensions is $\tau = [(d-1)D_r]^{-1}$, while $\tau = \alpha^{-1}$ for RTPs. The corresponding persistence length is given by $\ell_p = \mu f_p \tau$.

AOUPs have been introduced to model active particles whose propulsion forces have fluctuating norms. In this model, the active force evolves according to the following Ornstein-Uhlenbeck process:

$$\tau \dot{\mathbf{f}}_p = -\mathbf{f}_p + \frac{\sqrt{2D_{\mathrm{eff}}}}{\mu}\boldsymbol{\eta}. \tag{2}$$

In Eq. (2), $\boldsymbol{\eta}(t)$ is a centered Gaussian white noise of unit amplitude and independent components. This model was first studied long before active matter existed as a field, as one of the simplest models of diffusion with colored noise (Hänggi and Jung, 1994). In the context of active matter, AOUPs were independently introduced to model the dynamics of crawling cells (Sepúlveda *et al.*, 2013) and as a simplified model for which analytical progress is tractable (Szamel, 2014).[1] The Gaussian nature of the self-propelled force has indeed allowed a variety of problems to be analytically studied (Maggi, Marconi *et al.*, 2015; Fodor *et al.*, 2016; Berthier, Flenner, and Szamel, 2017; Wittmann, Maggi *et al.*, 2017; Wittmann, Marconi *et al.*, 2017; Woillez, Kafri, and Gov, 2020; Woillez, Kafri, and Lecomte, 2020; Martin *et al.*, 2021). For AOUPs, the persistence time is given by τ, while the typical propulsion force can be defined from $f_{\mathrm{p}}^2 = \langle \mathbf{f}_{\mathrm{p}}^2 \rangle = dD_{\mathrm{eff}}/(\mu^2\tau)$, where $\langle\cdot\rangle$ is an average over histories. The persistence length can then be computed as

$$\ell_{\mathrm{p}} \equiv \left\langle [\mathbf{r}(t)-\mathbf{r}(0)]\cdot\frac{\mathbf{f}_{\mathrm{p}}(0)}{|\mathbf{f}_{\mathrm{p}}(0)|}\right\rangle \underset{t\to\infty}{\sim} \mu\tau\langle|\mathbf{f}_{\mathrm{p}}(0)|\rangle = \sqrt{\frac{2D_{\mathrm{eff}}\tau}{\pi}}.$$

Despite their different dynamics, ABPs, RTPs, and AOUPs all lead to force autocorrelation functions that decay exponentially in time,

$$\langle f_{\mathrm{p},i}(t) f_{\mathrm{p},j}(0)\rangle = \delta_{ij}\frac{f_{\mathrm{p}}^2}{d}e^{-t/\tau}, \tag{3}$$

with $f_{\mathrm{p},k}$ denoting the spatial components of $\mathbf{f}_{\mathrm{p}}$. At large scales, all lead to diffusive dynamics with an effective diffusion coefficient $D_{\mathrm{eff}} = \mu^2 f_{\mathrm{p}}^2\tau/d$. For ABPs and RTPs, this can be written as $D_{\mathrm{eff}} = \ell_{\mathrm{p}}^2/(d\tau)$. For AOUPs, the scale of the active force is proportional to the number of space dimensions and the fluctuations of f_{p} lead to an extra contribution to the diffusivity such that $D_{\mathrm{eff}} = \pi\ell_{\mathrm{p}}^2/(2\tau)$.

Typical trajectories for the three types of particles are shown in Fig. 1 (top sketches), which highlights their differences on short length scales. While these differences are irrelevant at the scale of diffusive dynamics, they play an important role in the presence of external potentials. For example, in the large persistence regime it was predicted that RTPs (Tailleur and Cates, 2008, 2009; Basu *et al.*, 2020; Smith *et al.*, 2022) and ABPs (Hennes, Wolff, and Stark, 2014; Solon, Cates, and Tailleur, 2015; Malakar *et al.*, 2020) will accumulate away from the center of a confining harmonic well, and such an accumulation has indeed been observed experimentally (Takatori *et al.*, 2016; Schmidt *et al.*, 2021). On the contrary, in a harmonic potential AOUPs always have a steady state given by a centered Gaussian distribution (Szamel, 2014) and, somewhat surprisingly, their dynamics obey detailed balance (Fodor *et al.*, 2016).

[1]Other models of active particles have also been considered in the literature, for example, by considering underdamped Langevin equations with nonlinear friction (Romanczuk *et al.*, 2012). In some limits, they yield the standard ABP and RTP models.

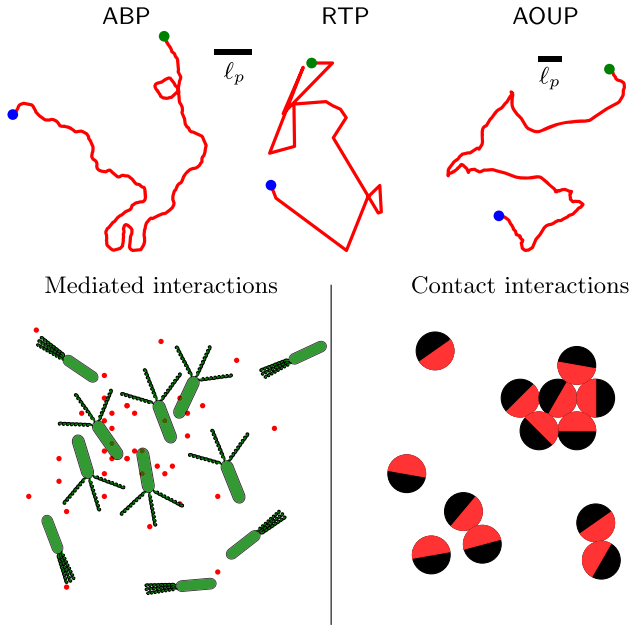

FIG. 1. Top sketches: representative trajectories for the three types of active particles described in Sec. II.A, all with the same persistence time $\tau = 1$, total duration $T = 20$, and effective diffusion coefficient $D_{\mathrm{eff}} = 1$. For ABP and RTP, this corresponds to $v_{\mathrm{p}} = \sqrt{2}$ and a persistence length $\ell_{\mathrm{p}} = \sqrt{2}$ that is indicated as a scale bar. For AOUP, it corresponds to a smaller $\ell_{\mathrm{p}} = \sqrt{2/\pi}$. The dark blue and light green dots indicate the starting and finishing positions, respectively. Bottom panels: schematic representation of mediated and contact interactions occurring between active particles.

B. Interacting scalar active matter

In this Colloquium, we focus on scalar active matter, i.e., on active systems whose long-time and large-scale behaviors are entirely captured by the stochastic dynamics of a density field. All dilute dry active systems fall into this class, as do a wealth of interacting ones.

A scalar theory generically describes systems where the interactions depend on and impact only the particle positions. For instance, this is the case for attractive or repulsive pairwise forces that play an important role in dense active systems (Fily and Marchetti, 2012; Redner, Hagan, and Baskaran, 2013; Stenhammar *et al.*, 2014, 2015; Wysocki, Winkler, and Gompper, 2014). It also applies to interactions that act only on the magnitude of the self-propulsion velocity and not on its direction (Liu *et al.*, 2011; D'Alessandro *et al.*, 2017). For instance, such interactions can be mediated by chemical signals as encountered in assemblies of cells interacting via "quorum sensing" (QS). This is depicted in Fig. 1 (bottom left panel), where the cells adapt their behavior to the concentration of diffusing signaling molecules. QS is generic in nature (Miller and Bassler, 2001) and plays an important role in diverse biological functions ranging from bioluminescence (Nealson, Platt, and Hastings, 1970; Engebrecht and Silverman, 1984; Fuqua, Winans, and Greenberg, 1994; Verma and Miyashiro, 2013) and virulence (Tsou and Zhu, 2010) to biofilm formation and swarming

(Hammer and Bassler, 2003; Daniels, Vanderleyden, and Michiels, 2004). It can also be engineered by genetic manipulation of bacteria (Liu *et al.*, 2011; Curatolo *et al.*, 2020) or using light-controlled colloids (Bäuerle *et al.*, 2018; Massana-Cid *et al.*, 2022). Integrating out the dynamics of the mediating chemical field, particles interacting via QS can be modeled by motility parameters that depend on the density field, for example, through a self-propulsion force $f_p(\mathbf{r}, [\rho])$ that is both a function of the position $\mathbf{r}$ and a functional of the density field $\rho(\mathbf{r})$ (Cates and Tailleur, 2015).

Note that many active systems also experience interactions that require more complex effective ("hydrodynamic") descriptions. For example, this is the case when the rotational symmetry of the system is spontaneously broken. The prototypical example is that of the Vicsek model (Vicsek *et al.*, 1995), where strong-enough aligning torques between the particles lead to the emergence of an ordered polar phase in dense systems (Marchetti *et al.*, 2013; Chaté, 2020). A proper hydrodynamic description of the corresponding flocking phase then requires the inclusion of the orientation field (Toner, Tu, and Ramaswamy, 2005). A wealth of other interactions may impact the particle's orientations, like chemotaxis (Berg, 2004), which preferably makes cells move up or down chemical gradients, or contact inhibition of locomotion (Stramer and Mayor, 2017) that may lead to cells reverting their directions of motion upon encounters. We stress that the disordered phases of all such systems nevertheless remain part of scalar active matter and already exhibit nontrivial collective behaviors; see Brenner, Levitov, and Budrene (1998), Saha, Golestanian, and Ramaswamy (2014), and O'Byrne and Tailleur (2020) for discussions of chemotactic interactions, see Sesé-Sansa, Pagonabarraga, and Levis (2018) for a discussion of polar alignment, and see Spera *et al.* (2023) for a discussion of nematic alignment.

C. Collective behavior in scalar active matter

In this section, we turn to the collective behaviors that are typically encountered in scalar active matter. When one considers systems whose large-scale behaviors are characterized by the conserved dynamics of a density field, the simplest possible phase transition corresponds to condensation and the breaking of translational uniformity.

In many active particle contexts, condensation has been theoretically predicted to arise from the interplay among attractive, repulsive, and propulsion forces (Fily and Marchetti, 2012; Mognetti *et al.*, 2013; Redner, Baskaran, and Hagan, 2013; Redner, Hagan, and Baskaran, 2013; Stenhammar *et al.*, 2014; Paliwal *et al.*, 2018; Spera *et al.*, 2023), and consistent behaviors have been experimentally reported using Janus self-propelled colloids (Theurkauff *et al.*, 2012; Buttinoni *et al.*, 2013; Palacci *et al.*, 2013; Liu *et al.*, 2019; van der Linden *et al.*, 2019). When self-propulsion is weak, attractive forces between the particles can easily overcome activity, and the expected equilibrium phase transitions typically survive. This is illustrated in Fig. 2 through numerical simulations of self-propelled ABPs in the presence of a translational noise and

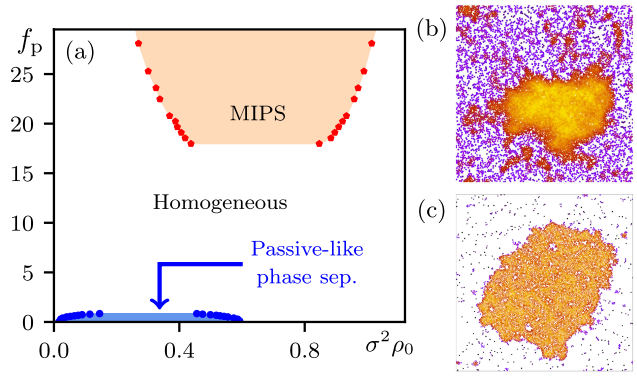

FIG. 2. Simulations of ABPs interacting via a Lennard-Jones potential: $V(r) = 4\epsilon[(\sigma/r)^{12} - (\sigma/r)^6]$ for $r < 2.7\sigma$, and $V(r) = 0$ otherwise. (a) Phase diagram obtained by varying f_p and the average density ρ_0. (b) Representative snapshot of the system in the MIPS region ($f_p = 42$ and $\rho_0 = 0.9$). (c) Representative snapshot of the system in the passivelike phase separation ($f_p = 0.4$ and $\rho_0 = 0.5$). The parameters are $\mu = 1$; translational diffusivity $D_t = 0.4$, rotational diffusivity $D_r = 2$, and $\sigma = 0.89$; and system size 300×300. Data courtesy of Gianmarco Spera.

Lennard-Jones interactions. At $f_p = 0$, the system undergoes equilibrium liquid-gas phase separation. As f_p increases, the phase-separated region shrinks until activity overcomes the attractive forces, and the system turns into a homogeneous fluid. Surprisingly, at even larger propulsion forces a reentrant phase transition into a phase-separated region is observed (Redner, Baskaran, and Hagan, 2013; Spera *et al.*, 2023).

The mechanism underlying this reentrant phase transition is MIPS, which is distinct from equilibrium phase separation and does not require attraction between the particles. Instead, MIPS results from the interplay between the tendency of active particles to accumulate where they move slower and their slowdown at high density due to collisions and repulsive forces (Cates and Tailleur, 2015).

MIPS has been reported in a wealth of active systems and can arise from a variety of interactions.

- Quorum sensing, when the self-propulsion speed decreases fast enough as the local density increases (Tailleur and Cates, 2008; Liu *et al.*, 2011; Cates and Tailleur, 2013; Bäuerle *et al.*, 2018; Curatolo *et al.*, 2020).
- Pairwise forces, as head-on collisions effectively reduce the particle self-propulsion speed (Fily and Marchetti, 2012; Redner, Hagan, and Baskaran, 2013; Stenhammar *et al.*, 2014; Wysocki, Winkler, and Gompper, 2014).
- Chemotaxis, in which the particles either slow down as they swim in the direction of decreasing density gradients or turn preferentially to face denser regions (O'Byrne and Tailleur, 2020; Zhang *et al.*, 2021; Zhao, Košmrlj, and Datta, 2023).
- Steric hindrance on lattice models (Thompson *et al.*, 2011; Whitelam, Klymko, and Mandal, 2018; Adachi and Kawaguchi, 2020; Shi *et al.*, 2020), where exact hydrodynamics equations (Kourbane-Houssene *et al.*, 2018), fluctuating hydrodynamics (Agranov *et al.*, 2021), and critical properties (Partridge and Lee,

2019; Dittrich, Speck, and Virnau, 2021; Maggi *et al.*, 2021) are more easily derived or characterized.

Much progress has been made in understanding and characterizing the emergence of MIPS using either direct coarse graining of microscopic models or phenomenological field theories, and many reviews on the topic exist in the literature (Cates and Tailleur, 2015; Fodor and Marchetti, 2018; Stenhammar, 2021; O'Byrne *et al.*, 2023). For completeness, the interested reader can find a discussion of the corresponding material as well as an overview of MIPS-related phenomena in the Appendix.

Thus far most results on the collective behaviors of scalar active matter have been established in idealized systems, invariant by translation and endowed with periodic boundary conditions. In equilibrium, when the correlation length is finite, obstacles and boundaries alter the system only in their immediate vicinity, which legitimates this approach. As we see in Sec. VI, the situation is much different for active systems, where boundaries may have a far-reaching influence on bulk behaviors. Before we discuss this case, we first review the anomalous mechanical forces exerted by active systems on boundaries and inclusions, which are at the root of this important difference between active and passive systems.

III. MECHANICAL FORCES ON CONFINING BOUNDARIES

In recent years, it has become evident that active systems display many anomalous properties when they interact with boundaries. Arguably the simplest demonstration of this is obtained by placing an asymmetric mobile partition in a cavity comprising a homogeneous gas of self-propelled ellipses. One then observes a spontaneous compression of one side of the system that is in apparent violation of the second law of thermodynamics[2]; see Fig. 3. By now it has become clear that such phenomena can be rationalized in terms of the anomalous mechanical properties of active fluids, which we review in this section.

A. Mechanical pressure on flat confining boundaries

Consider the simplest case of a two-dimensional gas of noninteracting active particles confined by a vertical flat wall localized at $x = x_{\mathrm{w}}$, which we model using a repulsive potential $V_{\mathrm{w}}(x)$ that vanishes for $x < x_{\mathrm{w}}$ and diverges at larger values of x. The pressure exerted by the gas on the wall can be computed as

$$P = \int_{x_b}^{\infty} dx\, \rho(x, y_b)\partial_x V_{\mathrm{w}}(x), \tag{4}$$

where $(x_b, y_b) \equiv \mathbf{r}_b$ corresponds to a point deep in the bulk of the active fluid, $x_b \ll x_{\mathrm{w}}$, and $\rho(\mathbf{r}, t) = \langle \sum_i \delta[\mathbf{r} - \mathbf{r}_i(t)] \rangle$ is the average number density; see Fig. 4. To determine P, we start from the dynamics of particle i, which reads

[2]This apparent violation of the second law is possible only because we describe here simply the active subsystem and not a closed system that would also include the energy source powering the active motion.

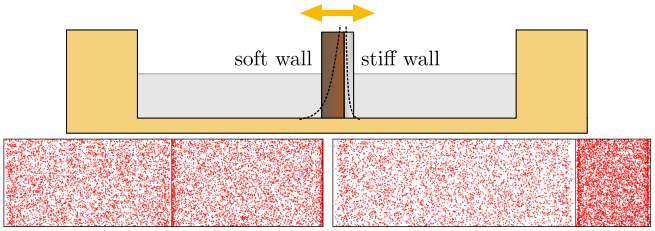

FIG. 3. Top sketch: a mobile partition that is stiffer on one side divides the system into two compartments, each initially with equal density. Since the pressure depends on the wall's stiffness through Eq. (20), each side of the partition experiences a different force from the active particles. As a result, the mobile partition moves until the forces on both sides balance. From Tailleur *et al.*, 2022. Bottom panels: numerical simulations corresponding to the setup described in the top panel using either circular ABPs (left panel) or elliptical ABPs (right panel). The absence of an equation of state (EOS) in the latter case is apparent from the spontaneous compression of one-half of the system. From Solon, Fily *et al.*, 2015.

$$\dot{\mathbf{r}}_i = \mu \mathbf{f}_{\mathrm{p}}^i - \mu \boldsymbol{\nabla} V_{\mathrm{w}}(\mathbf{r}_i) + \sqrt{2D_{\mathrm{t}}}\boldsymbol{\eta}_i, \tag{5}$$

where $\mathbf{f}_{\mathrm{p}}^i \equiv f_{\mathrm{p}}\mathbf{u}(\theta_i)$ is the particle propulsion force, μ is its mobility, D_{t} is a translational diffusivity, and $\boldsymbol{\eta}_i$ is a centered Gaussian white noise of unit variance. The evolution of ρ then satisfies a conservation law

$$\partial_t \rho(\mathbf{r}, t) = -\boldsymbol{\nabla} \cdot \mathbf{J}(\mathbf{r}, t), \tag{6}$$

where the current $\mathbf{J}$ is given by

$$\mathbf{J} = \mu \mathbf{F}_a(\mathbf{r}) - \mu\rho(\mathbf{r})\boldsymbol{\nabla} V_{\mathrm{w}}(\mathbf{r}) - D_{\mathrm{t}}\boldsymbol{\nabla}\rho(\mathbf{r}) \tag{7}$$

and $\mathbf{F}_a \equiv \langle \sum_i \mathbf{f}_{\mathrm{p}}^i \delta(\mathbf{r} - \mathbf{r}_i) \rangle$ is the active-force density. In the steady state, the confinement by a wall and the translational symmetry along the wall imply a vanishing current $\mathbf{J} = 0$. Using Eqs. (4) and (7), one can then write the pressure as

$$P = \frac{D_{\mathrm{t}}}{\mu}\rho(\mathbf{r}_b) + \int_{x_b}^{\infty} dx\, \mathbf{F}_a(x, y_b). \tag{8}$$

The pressure exerted by the system on the wall is thus the sum of the passive ideal-gas pressure and a contribution stemming from the active-force density, which is typically nonzero close to confining walls; see Fig. 4(d).

Before considering the case of self-propelled ellipses shown in Fig. 3, we start with the simpler case of ABPs that undergo isotropic rotational diffusion everywhere in space: $\dot{\theta}_i = \sqrt{2D_{\mathrm{r}}}\eta_i^{\mathrm{r}}$, where η_i^{r} is a centered Gaussian white noise of unit variance. To make progress, it is useful to introduce the active impulse of particle i, which is the average momentum the particle will receive in the future from the substrate on which it is pushing. For a circular ABP whose orientation is $\mathbf{u}[\theta_i(t)]$ at time t, the active impulse can be computed as

$$\Delta \mathbf{p}_i^a \equiv \int_t^{\infty} ds\, f_{\mathrm{p}} \overline{\mathbf{u}[\theta_i(s)]} = \frac{f_{\mathrm{p}}}{D_{\mathrm{r}}}\mathbf{u}[\theta_i(t)], \tag{9}$$

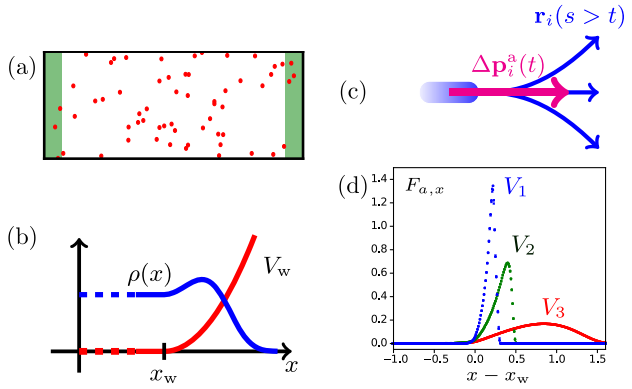

FIG. 4. (a) A simple setup to compute the pressure exerted by an active gas on confining walls consists of a 2D box with periodic boundaries along y and a confining potential along x. (b) Schematic representation of the density of active particles and of the confining wall potential shown in (a). (c) Despite the fact that the active force is doing an isotropic random walk, it will transmit a nonzero average momentum to the active particle between any time $s = t$ and $s = +\infty$. The corresponding "active" impulse $\Delta\mathbf{p}_i^a(t)$ (thicker arrow) is therefore nonzero. (d) The active-force densities measured for three different confining potentials are nonzero close to a confining wall. A clear dependence on the wall potential is shown. In the presence of an EOS, the areas under the three curves are the same.

where the overline denotes an average over future histories, i.e., over $\eta_i^r(s \geq t)$, and we have used $\overline{\mathbf{u}[\theta_i(s)]} = \mathbf{u}[\theta_i(t)]\exp[-D_r(s-t)]$. Even though the particle is undergoing a random walk so that its average active force is zero, the active impulse at time t is nonzero because of persistence; see Fig. 4(c). Direct aglebra then shows that the time evolution of the active impulse field $\Delta\mathbf{p}^a(\mathbf{r}) \equiv \langle\sum_i \Delta\mathbf{p}_i^a\delta(\mathbf{r}-\mathbf{r}_i)\rangle$ is given by

$$\partial_t\Delta\mathbf{p}^a(\mathbf{r}) = -\mathbf{F}_a(\mathbf{r}) + \boldsymbol{\nabla}\cdot\sigma_a(\mathbf{r}), \tag{10}$$

where

$$-\sigma_a \equiv \left\langle\sum_i \dot{\mathbf{r}}_i \otimes \Delta\mathbf{p}_i^a\delta(\mathbf{r}-\mathbf{r}_i)\right\rangle - D_t\boldsymbol{\nabla}\otimes\Delta\mathbf{p}^a(\mathbf{r}) \tag{11}$$

is a tensor that measures the flux of active impulse. In the homogeneous isotropic bulk of the system, a direct computation shows that $\sigma_a = -[\rho_b\mu f_p^2/(2D_r)]\mathbb{I}_d$, where $\mathbb{I}_d$ is the identity tensor. In the steady state, Eq. (10) shows that the density of active forces is the divergence of the "active stress tensor" σ_a,

$$\mathbf{F}_a(\mathbf{r}) = \boldsymbol{\nabla}\cdot\sigma_a(\mathbf{r}). \tag{12}$$

Equation (12) has a simple interpretation: the active impulse acts as a "momentum reservoir" for the particle. To produce a nonzero density of active force in a region of space, incoming and outgoing fluxes of active impulse have to differ. Finally, the pressure takes the ideal-gas law form

$$P = \rho(\mathbf{r}_b)\frac{D_t}{\mu} - \hat{\mathbf{x}}\cdot\sigma_a(\mathbf{r}_b)\cdot\hat{\mathbf{x}} = \rho_b T_{\text{eff}}, \tag{13}$$

where $\rho_b \equiv \rho(\mathbf{r}_b)$, $D_{\text{eff}} = D_t + (\mu f_p)^2/(2D_r)$ is the large-scale diffusivity of the particle, $T_{\text{eff}} \equiv D_{\text{eff}}/\mu$ is an effective temperature,[3] and $\hat{\mathbf{x}}$ is a unit vector in the x direction. The pressure can thus be written as the sum of a passive and an active stress, which is notable due to the absence of momentum conservation in the system. Since $\partial_t\langle\mathbf{r}_i\otimes\mathbf{u}_i\rangle = \langle\dot{\mathbf{r}}_i\otimes\mathbf{u}_i\rangle - D_r\langle\mathbf{r}_i\otimes\mathbf{u}_i\rangle$, one finds that in a homogeneous bulk the active stress tensor can be rewritten as

$$\sigma_a = -\left\langle\sum_i \mathbf{r}_i\otimes\mathbf{f}_p^i\delta(\mathbf{r}-\mathbf{r}_i)\right\rangle. \tag{14}$$

Equation (14) was introduced by Takatori, Yan, and Brady (2014), who called it the swim pressure. It can also be obtained using methods developed by Irving and Kirkwood (Yang, Manning, and Marchetti, 2014) or using a generalized virial theorem (Winkler, Wysocki, and Gompper, 2015; Falasco *et al.*, 2016).

Note that when the active-force density satisfies Eq. (12) there is a relation in the steady state between the total current $\mathbf{J}_{\text{tot}}$ flowing through the system and the total force $\mathbf{F}_{\text{tot}}$ exerted by the particles on the boundary. To see this, integrate Eq. (7) over space so that the total current $\mathbf{J}_{\text{tot}} \equiv \int d^2\mathbf{r}\mathbf{J}(\mathbf{r})$ satisfies

$$\mathbf{J}_{\text{tot}} = -\mu\int d^2\mathbf{r}\,\rho(\mathbf{r})\boldsymbol{\nabla}V_w(\mathbf{r}) \equiv -\mu\mathbf{F}_{\text{tot}}, \tag{15}$$

where we use $\int d^2\mathbf{r}\mathbf{F}_a(\mathbf{r}) = 0$ due to Eq. (12). A more intuitive derivation of this result can be obtained by summing Eq. (5) over all particles and averaging over the steady-state distribution. One then gets

$$\mathbf{J}_{\text{tot}} = \left\langle\sum_i \dot{\mathbf{r}}_i\right\rangle = -\mu\left\langle\sum_i \boldsymbol{\nabla}V_w(\mathbf{r}_i)\right\rangle = -\mu\mathbf{F}_{\text{tot}}, \tag{16}$$

where the sum of the active forces has vanished since the dynamics of the orientations are isotropic random walks decoupled from $\mathbf{r}_i(t)$ [which, as later elucidated, is the reason why Eq. (12) holds]. In flux-free systems, Eq. (16) thus implies that boundaries cannot exert any net total force on an active bath.

We note that Eq. (13) shows that the pressure is independent of the wall potential. This is noteworthy since $\mathbf{F}_a(\mathbf{r})$ depends on the choice of confining potential $V_w(\mathbf{r})$; see Fig. 4(d). The underlying reason for this is that, since the dynamics of the particle orientation is independent from all other degrees of freedom, the total active impulse that the particle can transfer to the wall does not depend on the wall potential. The existence of an equation of state for the pressure can be generalized to ABPs interacting via pairwise forces and can be used to derive a mechanical theory for MIPS in such systems (Takatori, Yan, and Brady, 2014; Solon, Stenhammar

[3]We note that, beyond the analogy with the ideal-gas law, T_{eff} does not generally play a thermodynamic role in active systems.

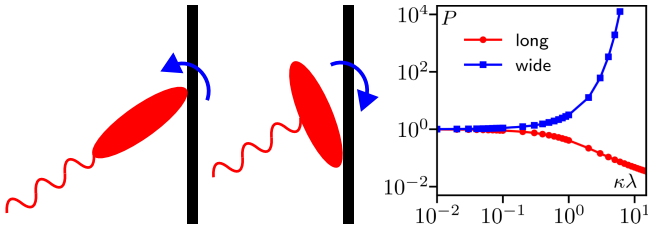

FIG. 5. Schematic representation of an elliptic active particle hitting a wall. Depending on the aspect ratio, the collision rotates the particle in opposite directions, making it face parallel or toward the wall. Right panel: mechanical pressure measured on the wall for noninteracting ABPs with an aspect-ratio parameter $\kappa = |a^2 - b^2|/8$, where a and b are the axis lengths of the ellipse. The wall is a confining harmonic potential of stiffness λ. The parameters are $f_p = \mu = 1$, $D_r = 0.5$, $\lambda = 1$, bulk density $\rho = 1$, and system size 20×2. As suggested by the left panel, the pressure exerted by long particles ($a > b$) is decreased by the wall torques, whereas that exerted by wide particles ($a < b$) is enhanced.

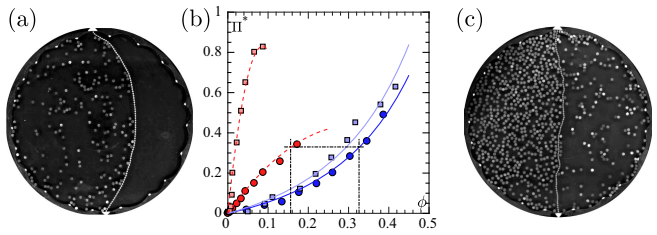

FIG. 6. (a) A flexible chain separates a system of vibrated grains into two cavities. The chain curvature is used to measure the pressure exerted by the particles confined in the left cavity, which can be either isotropic passivelike disks or anisotropic active disks. (b) Pressure Π measured as the packing fraction ϕ is varied. For isotropic disks (blue, close to solid lines), Π is in agreement with the equilibrium equation of states for hard disks (plain lines). For active disks (red, close to dashed lines), two types of chains made with links of different sizes measure different pressures (squares and circles), signaling the absence of an equation of state for the pressure. The dot-dashed lines denote positions where active and passive disks are in equilibrium at different densities, as shown in (c). From Junot *et al.*, 2017.

et al., 2015; Solon *et al.*, 2018a, 2018b; Speck, 2021; Omar *et al.*, 2023).

We note, however, that the derivation of Eq. (13) does not account for the simulations reported in Fig. 3. One thus needs to go one step further and account for the ellipsoidal particle shapes by considering the torques Γ exerted by the walls on the particles: $\dot{\theta}_i = \Gamma(\mathbf{r}_i, \theta_i) + \sqrt{2D_r}\eta_i^r$. In this case, the time evolution of the active-force density $\mathbf{F}_a(\mathbf{r})$ is given by

$$\partial_t \mathbf{F}_a(\mathbf{r}) = \left\langle \sum_i f_p \Gamma(\mathbf{r}_i, \theta_i)\mathbf{u}^\perp(\theta_i)\delta(\mathbf{r} - \mathbf{r}_i) \right\rangle - D_r \mathbf{F}_a(\mathbf{r}) - \nabla \cdot \left[\left\langle \sum_i \dot{\mathbf{r}}_i \otimes \mathbf{f}_p^i \delta(\mathbf{r} - \mathbf{r}_i) \right\rangle \right], \tag{17}$$

where $\mathbf{u}^\perp(\theta) = \partial_\theta \mathbf{u}(\theta)$. In the steady state, one finds that

$$\mathbf{F}_a(\mathbf{r}) = \boldsymbol{\nabla} \cdot \sigma_a^{\mathrm{tf}} + \left\langle \sum_i \frac{f_p}{D_r} \Gamma(\mathbf{r}_i, \theta_i)\mathbf{u}^\perp(\theta_i)\delta(\mathbf{r} - \mathbf{r}_i) \right\rangle, \tag{18}$$

where $\sigma_a^{\mathrm{tf}} = -\langle \sum_i \dot{\mathbf{r}}_i \otimes (\mathbf{f}_p^i/D_r)\delta(\mathbf{r} - \mathbf{r}_i)\rangle$ is the flux of active impulse in the absence of torques. Equation (18) thus splits the contribution to the density of active forces between conserved and nonconserved parts, hence showing that wall-induced torques can be seen as sources or sinks of active impulse. When $\psi(\mathbf{r}, \theta) = \langle \sum_i \delta(\mathbf{r} - \mathbf{r}_i)\delta(\theta - \theta_i)\rangle$ is introduced, the pressure can be written as

$$P = \rho_b T_{\mathrm{eff}} + \Delta P_w, \tag{19}$$

where ΔP_w is a wall-dependent contribution given by

$$\Delta P_w = \frac{\mu f_p}{D_r} \int d\theta \int_{x_b}^{\infty} dx\, \psi(x, y_b, \theta)\Gamma(x, y_b, \theta) \sin\theta. \tag{20}$$

Note that the pressure is no longer independent of the wall, which explains the spontaneous compression of the asymmetric piston shown in Fig. 3. Indeed, the piston is stalled when the pressures on both sides are equal, which requires $\Delta P_{w_L}(\rho_L) = \Delta P_{w_R}(\rho_R)$. When the left and right walls of the piston are different, this equality requires different densities on the two sides of the piston.

The previous discussion can be understood by thinking about the most commonly encountered active particles around us: pedestrians. Think about a small child running toward you. Stopping the child requires one to make its translational speed vanish, hence bringing the corresponding incoming momentum flux to zero. This corresponds to the drop of the passive momentum ($\rho D_t/\mu$ in the case of an ideal gas). If the child keeps running while you are holding them, you have to absorb an additional momentum flux that the child is transferring from the ground onto you, which corresponds to the contribution of the active force in Eq. (8). Because many different strategies can be employed to stop the child from running, the active pressure will generically depend on the restraining adult, hence leading to the lack of an equation of state. This is how torques lead to a lack of equation of state, as illustrated in Fig. 5. For torque-free ABPs, because the dynamics of the active force is independent of all other degrees of freedom, the momentum flux they transfer to the wall through their active force before running away is always given by $\mu f_p^2/(2D_r)$, which leads to an equation of state. We note that this is an idealized limit and that, for dry active systems, the lack of an equation of state is expected to be generic, a fact that has been confirmed experimentally (Junot *et al.*, 2017) for self-propelled disks; see Fig. 6. We stress that the lack of an equation of state is not necessarily related to torques induced by confining walls. Aligning interactions and motility regulation have, for instance, also been shown to prevent the existence of an equation of state for the pressure (Solon, Fily *et al.*, 2015).

B. Curved and flexible boundaries

The anomalous mechanical properties of dry active systems are not restricted to the lack of an equation of state for flat walls. Indeed, even in cases where an equation of state exists,

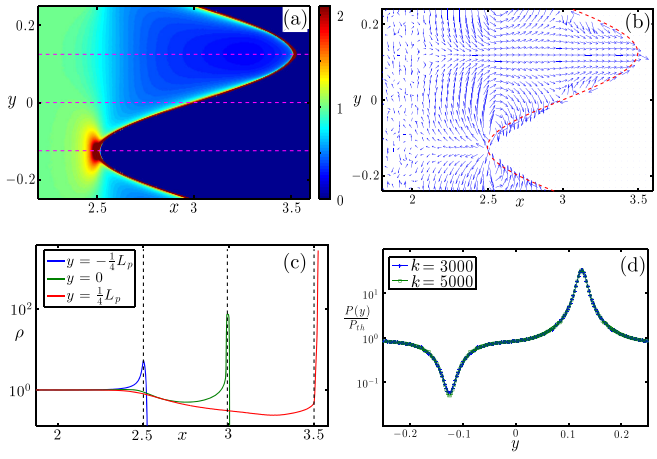

FIG. 7. (a) Density and (b) current of noninteracting ABPs near the right edge of the system with the curved-wall potential given in Eq. (21). The parameters are $f_p = D_r = 24$, $D_t = 0$, $L_p = 0.5$, $A = 0.5$, $k = 10^3$, $x_0 = 3$, and $\mu = 1$. The dashed red curve corresponds to $x_w(y)$. (c) Cross sections of the particle density taken at the three horizontal dashed lines in (a). The vertical lines correspond to $x_w(y)$. (d) Pressure normal to the wall, normalized by Eq. (13), as a function of y in the hard-wall limit. From Nikola *et al.*, 2016.

the local pressure exerted by active fluids on confining walls generically depends on the boundary shape (Fily, Baskaran, and Hagan, 2014; Mallory, Valeriani, and Cacciuto, 2014; Fily, Baskaran, and Hagan, 2015; Yan and Brady, 2015; Nikola *et al.*, 2016). This can be traced back to the fact that, after colliding with a wall, active particles glide along it and accumulate in regions with higher curvatures (Fily, Baskaran, and Hagan, 2014; Mallory, Valeriani, and Cacciuto, 2014) in a manner that depends on their size and shape (Wysocki, Elgeti, and Gompper, 2015). This leads to nontrivial density modulations and currents near the wall (Fily, Baskaran, and Hagan, 2014, 2015; Mallory, Valeriani, and Cacciuto, 2014; Yan and Brady, 2015) that are illustrated in Fig. 7 using numerical simulations of ABPs interacting with a periodic soft-wall potential that vanishes for $x < x_w$ and is otherwise given by

$$V(\mathbf{r}) = \frac{k}{2}[x - x_w(y)]^2, \tag{21}$$

with $x_w(y) = x_0 + A\sin(2\pi y/L_p)$ and L_p the period. Note that Fig. 7(d) shows that the pressure, measured as the force normal to the wall, depends on the exact location along the wall.

The difference between the point of highest pressure and lowest pressure δP is found numerically to be proportional to the curvature $1/R$ at the tips of the sinusoidal wall; see Fig. 8. This is consistent with measurements of the pressure exerted by an active ideal gas on a 2D circular cavity of radius R (Mallory *et al.*, 2014; Smallenburg and Löwen, 2015; Yan and Brady, 2015; Sandford, Grosberg, and Joanny, 2017). Moreover, recently the corresponding finite-size correction was computed analytically and shown to be given by (Zakine *et al.*, 2020)

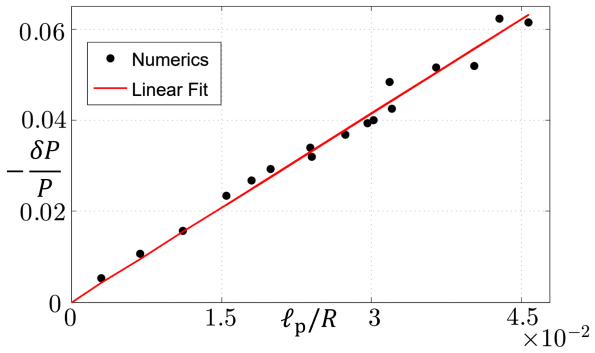

FIG. 8. Difference δP between the pressure at the concave and convex apices of the curved-wall potential given in Eq. (21), as the radius of curvature $R = L_p/(4\pi^2 A)$ is varied. The red line is a linear fit of the data leading to a slope ∼1.3. Numerical data were obtained using simulations of ABPs with $f_p = 0.75$ and $\mu = D_r = 1$. Wall parameters in the ranges $A \in [3.1 \times 10^{-3}, 3.3 \times 10^{-2}]$ and $L_p \in [3.6, 5.5]$ were used, with $k = 2 \times 10^4$. Assuming $\gamma \simeq -P/\ell_p$ on dimensional ground and using the generalized Laplace law predicts a slope of 2. From Nikola *et al.*, 2016.

$$P(R) = P_b - \frac{\gamma}{R} + o(R^{-1}), \tag{22}$$

where $P_b = \rho_b T_{\text{eff}}$ is the pressure in an infinite system at density ρ_b and γ is the fluid-solid surface tension. The latter can be computed as an integral over the density profile $\rho(r)$ normal to the curved interface[4]

$$\gamma \equiv \int_0^R dr \frac{\mu}{2} f_p^2 \tau \rho_b - \int_0^\infty dr \frac{\mu}{2} f_p^2 \tau \rho(r). \tag{23}$$

Equation (23), which generalizes Laplace's law to active fluids, directly suggests that $\delta P \simeq 2\gamma/R$. On dimensional grounds, one can estimate the surface tension as $\gamma \simeq -P_b \ell_p$, with ℓ_p the persistence length. This agrees semiquantitatively with the measurements shown in Fig. 8. As shown in Eq. (23), the negative sign of γ is due to the tendency of active particles to accumulate at the wall. It is consistent with the overall sign of δP, which can also be understood heuristically, as the active particles accumulate at concave regions of the wall. Note that the sign of δP shows that active particles tend to exert forces on curved boundaries that would amplify the deformation of a flexible boundary, as later discussed.

For walls that are not reflection symmetric, a net shearing force develops parallel to the wall (Nikola *et al.*, 2016). This can be understood as a consequence of the ratchet effect (Angelani, Costanzo, and Di Leonardo, 2011; Reichhardt and Reichhardt, 2013; Ai and Wu, 2014): The breaking of time-reversal symmetry by the active particles coupled to a breaking of an inversion symmetry leads to a steady-state current along the wall; see Reichhardt and Reichhardt (2017) for a review. In turn, Eq. (7) tells us that such a current will generically be associated with a force tangential to the wall.

[4]Note that, for an equilibrium passive ideal gas at temperature T, the fluid-solid surface tension is also given by Eq. (23) upon replacing $(\mu/2)f_p^2\tau$ with $k_B T$ (Zakine *et al.*, 2020).

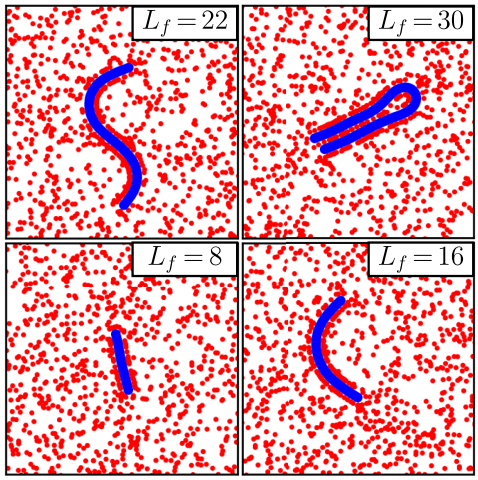

FIG. 9. Typical configurations of semiflexible filaments of length L_f in a bath of active Brownian particles. An instability develops for long enough filaments. Adapted from Nikola *et al.*, 2016.

This explains the spontaneous rotation of microscopic gears observed in simulations (Angelani, Di Leonardo, and Ruocco, 2009) and experiments (Di Leonardo *et al.*, 2010; Sokolov *et al.*, 2010).

The dependence of the active pressure on the boundary shape is exemplified by considering the behavior of flexible elastic objects inside an active fluid. For concreteness, first consider a flexible partition whose ends are held at walls at the top and bottom of a container filled with active particles. Once a fluctuation creates a local deformation in the filament, Eq. (22) suggests that a finite pressure difference $\Delta P \simeq 2\gamma/R$ develops between its two sides, with R the radius of curvature at the apex of the deformation. This tends to increase the deformation and is opposed by the elasticity of the flexible partition. The outcome of this competition can be understood by considering the linearized dynamics of the partition, which are characterized by a Monge representation $h(x,t)$. Because the accumulation of active particles is proportional to the curvature of the confining interface (Fily, Baskaran, and Hagan, 2014; Nikola *et al.*, 2016), one expects $\Delta P \propto \boldsymbol{\nabla}^2 h$, leading to (Nikola *et al.*, 2016)

$$\partial_t h(x,t) = (T - 2\gamma)\boldsymbol{\nabla}^2 h(x,t) - \kappa_b \boldsymbol{\nabla}^4 h(x,t), \qquad (24)$$

where T and κ_b are the line tension and bending rigidity, respectively. Equation (24) shows that, for large activity when $2\gamma > T$, a horizontal filament is unstable to fluctuations above a characteristic length $\lambda \propto \sqrt{\kappa_b/(2\gamma - T)}$. For short filaments, one thus expects the rigidity to keep the filament straight, whereas long filaments are expected to be unstable. This has indeed been observed in both simulations and experiments (Nikola *et al.*, 2016; Junot *et al.*, 2017), where the instability has been shown to coarsen and lead to a deformation of the filament with a wavelength set by the system size. For an unpinned passive flexible filament in an active medium, an even richer scenario has been reported in both simulations and experiments (Nikola *et al.*, 2016; Anderson *et al.*, 2022); see Fig. 9. As the length of the filament increases, the previously discussed instability first leads to a left-right asymmetry and the spontaneous formation of a parachutelike structure (Harder, Valeriani, and Cacciuto, 2014; Shin *et al.*, 2015) that is somewhat reminiscent of a sail blowing in the wind, except with the wind itself generated by the curving filament. The pressure difference on the two sides of the filament then generates a net propelling force and turns the filament into an emergent active particle. Upon a further increase in length, a full period of the unstable mode develops, leading to short-lived spontaneous rotors. Finally, long filaments are found to lead to folded structures.

C. Summary

In this section, we have seen how the pressure of scalar active fluids exhibits markedly different properties from that of passive ones. The generic lack of an equation of state is probably the most striking difference. It leads to atypical behaviors such as the spontaneous compression of an asymmetric piston inserted into a uniform fluid. Predicted using idealized models of active particles, this lack of an equation of state has been confirmed experimentally using vibrated disks. We have shown how the lack of an equation of state can be related to a history-dependent average active force experienced by the particles. On the contrary, when the active-force dynamics is independent from the other degrees of freedom, an equation of state is recovered. Even in this case, a rich physics is reported in the presence of curved or flexible boundaries.

IV. OBSTACLES AND LOCALIZED INCLUSIONS

An even richer physics has been reported when considering the mechanical interplay between active particles and obstacles immersed in active fluids. Arguably the first observation of this was the experimental study of *asymmetric obstacles* by Galajda *et al.* (2007), who demonstrated that an array of V-shaped obstacles placed in a bacterial bath leads to the accumulation of bacteria on one side of the array; see Fig. 10. In this section, we discuss how a mechanical perspective accounts for the induced organization of the bacterial fluid and how to account for more general situations. In particular, we focus on the universal aspects of the large-scale density modulation and current induced by obstacles, and not on the rich physics that can be observed in the near field, at distances $\mathcal{O}(\ell_p)$ from the obstacle, which has attracted significant attention (Kaiser, Wensink, and Löwen, 2012; Potiguar, Farias, and Ferreira, 2014; Ni, Cohen Stuart, and Bolhuis, 2015; Zaeifi Yamchi and Naji, 2017; Yan and Brady, 2018; Wysocki and Rieger, 2020; Speck and Jayaram, 2021) and has already been reviewed (Bechinger *et al.*, 2016).

We start with the case of a single obstacle immersed in an infinite active fluid and show how a multipole expansion allows one to predict the far-field structure of density and current fields. A simple picture emerges in which the local asymmetry of the obstacle induces a ratchet current that mass conservation turns into long-range density and current modulations. Mathematically the relation between the force monopole exerted by the obstacle on the active fluid and the induced current flow is identical to that between

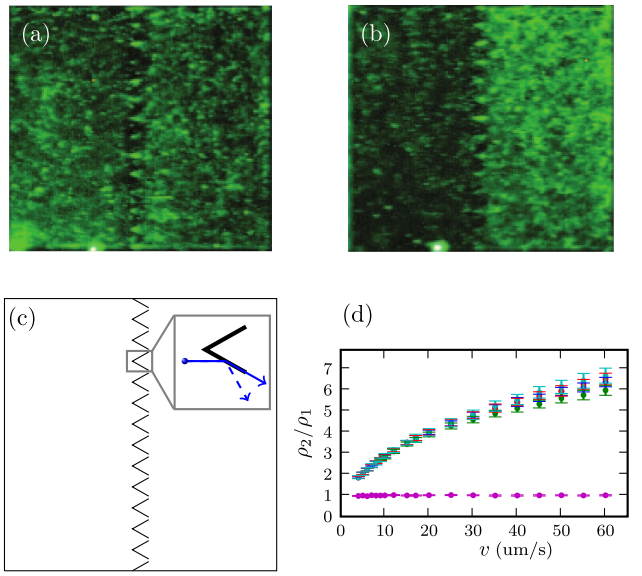

FIG. 10. A uniform density of bacteria at the beginning of the experiment (a) becomes inhomogeneous at late times (b) in a 2D microfluidic chamber split into two compartments by an array of asymmetric obstacles, as schematically depicted in (c). (d) Ratio between the densities of bacteria in the right (ρ_2) and left (ρ_1) sides of the cavity shown in (c) measured using numerical simulations of RTPs whose self-propulsion speed v is varied. All dimensions match the experiment: the enclosures dimensions are $L \times H = 400 \times 400$ μm^2, the arms of the funnels are 27 μm long and their apex angle is $\pi/3$, and the funnels are separated by gaps that are 3.8 μm wide. The tumbling rate of the RTPs is set to $\alpha = 1$ s^{-1}. The overlapping red, blue, green, and cyan symbols marking $\rho_2/\rho_1 > 1$ are obtained by varying H and the left and right chamber widths L_L and L_R, respectively, with $(L_R, L_L, H) \in \{(200, 200, 400), (400, 400, 400), (200, 200, 800), (400, 200, 400)\}$. The vertical density of obstacles is kept constant. The rectification of bacterial density is thus independent of finite-size effects. In all simulations, RTPs align with the walls upon collision [the solid line inside the inset of (c)]. When the RTPs instead experience specular reflection upon collision, as shown by the dashed line inside the inset of (c), a uniform density field is measured (the magenta symbols at $\rho_2/\rho_1 \simeq 1$). This is consistent with the fact that collisions are the sole irreversible process in these simulations. (a),(b) From Galajda *et al.*, 2007. (c),(d) From Tailleur and Cates, 2009.

electrostatic dipoles and fields. Next we turn to consider the effect of boundary conditions and show how an image theorem allows the results to be generalized to simple cases like periodic or closed boundary conditions. We then discuss how this leads to long-range nonreciprocal interactions between inclusions in an active fluid. Finally, we discuss the case of mobile inclusions and review recent work on passive tracers and the possible dynamics arising from interactions mediated by active baths.

A. A single obstacle in an infinite system

We consider N noninteracting ABPs in the presence of an obstacle modeled by an external potential $V(\mathbf{r})$ that is localized on a compact support near $\mathbf{r} = 0$. In d space dimensions, the average number density of particles $\mathcal{P}(\mathbf{r}, \mathbf{u})$ at position $\mathbf{r}$ with an orientation $\mathbf{u}$ evolves according to

$$\partial_t \mathcal{P}(\mathbf{r}, \mathbf{u}) = -\boldsymbol{\nabla} \cdot [\mu f_p \mathbf{u} \mathcal{P} - \mu \mathcal{P} \boldsymbol{\nabla} V - D_t \boldsymbol{\nabla} \mathcal{P}] + D_r \Delta_{\mathbf{u}} \mathcal{P}, \tag{25}$$

where $\Delta_{\mathbf{u}}$ is the spherical Laplacian. Integrating over the orientation $\mathbf{u}$ leads to Eqs. (6) and (7), with V_w replaced by V.

Far from the obstacle, i.e., when $|\mathbf{r}| \gg \ell_p$, the active dynamics is diffusive at large scales such that $\mathbf{J} \simeq \mathbf{J}_D \equiv -D_{\text{eff}} \boldsymbol{\nabla} \rho$, where $D_{\text{eff}} = D_t + (\mu f_p)^2/(dD_r)$ (Cates and Tailleur, 2013). In the steady state, one has $\boldsymbol{\nabla} \cdot \mathbf{J} = 0 \simeq \boldsymbol{\nabla} \cdot \mathbf{J}_D$ so that the density profile solves the source-free Poisson equation $D_{\text{eff}} \boldsymbol{\nabla}^2 \rho = 0$. This is valid only far from the obstacle, where $\mathbf{J} \simeq \mathbf{J}_D$. On the contrary, close to the obstacle the current deviates from its diffusive approximation and we thus introduce

$$\delta \mathbf{J} \equiv \mathbf{J} - \mathbf{J}_D = \mu \mathbf{F}_a - \mu \rho \boldsymbol{\nabla} V + (D_{\text{eff}} - D_t) \boldsymbol{\nabla} \rho \tag{26}$$

to measure the difference between $\mathbf{J}$ and $\mathbf{J}_D$. To quantify the impact of the obstacle on the equation for ρ, we note that the steady-state equation $\boldsymbol{\nabla} \cdot \mathbf{J} = 0$, can be exactly rewritten as

$$D_{\text{eff}} \boldsymbol{\nabla}^2 \rho = \boldsymbol{\nabla} \cdot \delta \mathbf{J}(\mathbf{r}). \tag{27}$$

As stated, $\delta \mathbf{J}$ vanishes far from the obstacle and one recovers a source-free Poisson equation in the bulk. Equation (27) then shows that the obstacle simply leads to a source term $\boldsymbol{\nabla} \cdot \delta \mathbf{J}(\mathbf{r})$ localized in its vicinity. When the boundary condition at infinity is $\rho(\mathbf{r}) = \rho_b$, its solution is

$$\rho(\mathbf{r}) = \rho_b + \frac{1}{D_{\text{eff}}} \int d^d \mathbf{r}' G(\mathbf{r}, \mathbf{r}') \boldsymbol{\nabla} \cdot \delta \mathbf{J}(\mathbf{r}'), \tag{28}$$

where $G(\mathbf{r}, \mathbf{r}')$ is the Green's function of the Laplacian in d space dimensions.

To proceed, we use Eq. (26) to determine the leading contribution in $\delta \mathbf{J}(\mathbf{r}')$ to the density profile. To do so, we employ a multipole expansion of Eq. (28) in the far-field limit $|\mathbf{r}| \gg \ell_p$. Using Eqs. (12) and (26), one sees that the leading-order contribution is given by $\delta \mathbf{J}(\mathbf{r}') \simeq -\mu \rho(\mathbf{r}') \boldsymbol{\nabla} V(\mathbf{r}')$. Introducing the force monopole

$$\mathbf{p} = -\int d^d \mathbf{r}' \rho(\mathbf{r}') \boldsymbol{\nabla} V(\mathbf{r}') \tag{29}$$

and explicitly carrying out the multipole expansion of Eq. (28), one then finds that the leading-order far-field density and current are given by

$$\rho(\mathbf{r}) = \rho_b + \frac{\beta_{\text{eff}}}{S_d} \frac{\mathbf{r} \cdot \mathbf{p}}{r^d} + \mathcal{O}(r^{-d}), \tag{30}$$

$$\mathbf{J}(\mathbf{r}) = \frac{\mu}{S_d} \frac{d(\hat{\mathbf{r}} \cdot \mathbf{p})\hat{\mathbf{r}} - \mathbf{p}}{r^d} + \mathcal{O}(r^{-(d+1)}), \tag{31}$$

where $\beta_{\text{eff}} \equiv 1/T_{\text{eff}} = \mu/D_{\text{eff}}$ and $S_d = 2\pi^{d/2}/\Gamma(d/2)$. As usual with multipole expansions, Eq. (30) is the solution of

$$D_{\text{eff}}\nabla^2\rho = \nabla\cdot[\mu\mathbf{p}\delta(\mathbf{r})]. \tag{32}$$

We note that Eqs. (30) and (31) predict a universal density modulation and current induced by an obstacle that exerts a nonvanishing force monopole $\mathbf{p}$ on the active fluid. The determination of $\mathbf{p}$, however, depends on the details of the problem and requires an explicit derivation of the microscopic structure of $\rho(\mathbf{r})$ in the vicinity of the obstacle. This is in general a difficult problem with few exact results (Arnoulx de Pirey and van Wijland, 2023). We note that if $\mathbf{p}=0$, higher orders in the multipole expansion have to be considered (Baek *et al.*, 2018). When the obstacle is spherical, the density modulation and current vanish at all orders in the multipole expansion.

The aforementioned derivation shows how forces exerted by obstacles lead to large-scale ratchet currents. Note that, independently of the previously presented multipole expansion, we can derive an exact relation between the total current flowing through the system and the net force $\mathbf{p}$ exerted by the obstacle. Integrating the exact microscopic expression of the current field [Eq. (7)] over the full space indeed leads to

$$\mathbf{J}_{\text{tot}} \equiv \int d^d\mathbf{r}\,\mathbf{J}(\mathbf{r}) = \mu\mathbf{p}, \tag{33}$$

where we have used $\mathbf{F}_a(\mathbf{r}) = \nabla\cdot\sigma_a$ since the pressure admits an equation of state, and the active-force density can thus be written as the divergence of a local stress tensor. We note that all exact gradients entering the expression of $\mathbf{J}$ vanish upon integration due to the divergence theorem. This result is the direct counterpart to Eq. (16) for the case of an isolated obstacle.

While this formulation pertained to noninteracting ABPs, the result generalizes to homogeneous active fluids with pairwise interparticle forces (Granek *et al.*, 2020).

B. Finite systems and boundary conditions

Thus far we have considered the case of an isolated object in an infinite system and have shown that asymmetric obstacles induce long-range density modulations and currents. In turn, this implies that some care has to be taken when finite systems of linear size L are considered, even when $L \gg \ell_{\text{p}}$. We now discuss several such scenarios that have been explored in the literature.

For periodic boundary conditions, when $L \gg \ell_{\text{p}}$ one can show that the system is equivalent to an infinite periodic lattice of obstacles (Granek *et al.*, 2020). The density and current fields, as well as the value of the force monopole $\mathbf{p}$, differ between infinite and periodic systems by corrections of the order of $\mathcal{O}(L^{-(d+2)})$ (Speck and Jayaram, 2021). For $L \lesssim \ell_{\text{p}}$, the far-field expansion is naturally invalid. Numerical simulations and a scaling argument reveal that for $d=2$ the force monopole $\mathbf{p}$ grows as $\sim L^2$ until it saturates at an asymptotic value for $L \gg \ell_{\text{p}}$ (Speck and Jayaram, 2021).

Another scenario that was considered is the effect of confining flat hard walls. The derivation of Sec. IV.A can be extended to this case (despite nontrivial boundary conditions) and, for a single obstacle displaced by $\mathbf{X} = X\hat{\mathbf{x}}$ from a hard wall at $x=0$, Eq. (28) still holds in the far field of both the obstacle and the wall (Ben Dor, Kafri *et al.*, 2022). The Green's function G is, however, replaced by that of the Laplacian in a half plane. To leading order in the limit $|\mathbf{r}-\mathbf{X}| \gg \ell_{\text{p}}$ and $X \gg \ell_{\text{p}}$, the solution is given by

$$\rho(\mathbf{r}) = \rho_b + \frac{\beta_{\text{eff}}}{S_d}\left[\frac{(\mathbf{r}-\mathbf{X})\cdot\mathbf{p}}{|\mathbf{r}-\mathbf{X}|^d} + \frac{(\mathbf{r}-\mathbf{X}^*)\cdot\mathbf{p}^*}{|\mathbf{r}-\mathbf{X}^*|^d}\right] + \mathcal{O}(|\mathbf{r}-\mathbf{X}|^{-d}, X^{-d}), \tag{34}$$

where $\mathbf{p}^*$ and $\mathbf{X}^*$ are the images of $\mathbf{p}$ and $\mathbf{X}$ with respect to the wall, respectively. Note that Eq. (34) holds with the force monopole $\mathbf{p}$ given by its infinite-system value. Indeed, the corrections to $\mathbf{p}$ due to the image obstacle enter at order $\mathcal{O}(X^{-(d-1)})$. Equation (34) was also shown to hold when the obstacle was on the wall so that $\mathbf{X}=0$, with $\mathbf{p}$ parallel to the wall (Ben Dor, Ro *et al.*, 2022). Finally, the derivation was also carried out for a circular cavity, as discussed in Sec. IV.E.

C. Nonreciprocal mediated interactions

Since isolated obstacles create long-range density modulations, it is natural to expect that several obstacles immersed in the same active fluid will experience long-range mediated interactions. These turn out to be *nonreciprocal* and can be derived as follows. Consider two obstacles $O^{(1)}$ and $O^{(2)}$ fixed at positions $\mathbf{X}^{(1)}$ and $\mathbf{X}^{(2)}$, respectively, and denote by $\mathbf{r}_{12}$ their separation; see Fig. 11. The effect of $O^{(1)}$ on $O^{(2)}$ can be quantified by an emergent interaction force $\mathbf{F}_{12}$, which can be identified as the net residual force exerted on $O^{(2)}$ due to the introduction of $O^{(1)}$ into the bath,

$$\mathbf{F}_{12} \equiv \mathbf{p}_2^0 - \mathbf{p}_2, \tag{35}$$

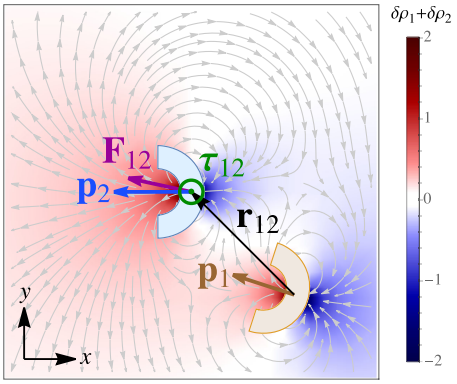

FIG. 11. Schematic diagram of two interacting asymmetric passive obstacles in two dimensions. Obstacle $O^{(1)}$ (orange, bottom right) is placed at $\mathbf{X}_1$, obstacle $O^{(2)}$ (blue, center) is placed at $\mathbf{X}_2$, and we denote their separation by $\mathbf{r}_{12}$. The color map, which has negative values on the convex part of the obstacles and positive values on the concave part, shows the superposed far-field single-body density modulations $\delta\rho_1+\delta\rho_2$, with $\delta\rho_n = \beta_{\text{eff}}(\mathbf{r}-\mathbf{X}_n)\cdot\mathbf{p}_n/(2\pi|\mathbf{r}-\mathbf{X}_n|^2)$. The corresponding currents $\mathbf{J}_1+\mathbf{J}_2$ and $\mathbf{J}_n = -D_{\text{eff}}\nabla\delta\rho_n$ are shown as gray streamlines. The parameters are $D_{\text{eff}}=\beta_{\text{eff}}=1$, $\mathbf{X}_1=(4,-4)$, $\mathbf{X}_2=(0,0)$, $\mathbf{p}_1 = 0.5(\cos(11\pi/10), \sin(11\pi/10))$, and $\mathbf{p}_2 = (-0.5, 0)$. From Granek *et al.*, 2020.

where $-\mathbf{p}_k \equiv \int d^d\mathbf{r}\,\rho(\mathbf{r})\boldsymbol{\nabla}V_k(\mathbf{r}-\mathbf{X}^{(k)})$ is the net force exerted by the active bath on $O^{(k)}$ and $\mathbf{p}_2^0 = \mathbf{p}_2|_{V_1=0}$ is the force on $O^{(2)}$ in the absence of $O^{(1)}$. Inspection of Eq. (29) shows that $\mathbf{F}_{12}$ is directly connected to the density modulation induced by $O^{(1)}$ in the vicinity of $O^{(2)}$. For large separations $\mathbf{r}_{12}$, the leading-order contribution of this modulation is a local shift of the average density,

$$\delta\rho_1(\mathbf{X}_2) = \frac{\beta_{\mathrm{eff}}}{S_d}\frac{\mathbf{r}_{12}\cdot\mathbf{p}_1}{r_{12}^d} + \mathcal{O}(r_{12}^{-d}). \tag{36}$$

Owing to the linearity of Eq. (28), the force monopole exerted by $O^{(2)}$ is modified as

$$\mathbf{p}_2 = \frac{\rho_b + \delta\rho_1(\mathbf{X}_2)}{\rho_b}\mathbf{p}_2^0. \tag{37}$$

Inserting Eq. (37) into Eq. (35) results in

$$\mathbf{F}_{12} = -\frac{\beta_{\mathrm{eff}}}{S_d}\frac{\mathbf{r}_{12}\cdot\mathbf{p}_1^0}{\rho_b r_{12}^d}\mathbf{p}_2^0 + \mathcal{O}(r_{12}^{-d}), \tag{38}$$

where $\mathbf{p}_k = \mathbf{p}_k^0 + \mathcal{O}(r_{12}^{-(d-1)})$ and $\mathbf{p}_1^0 = \mathbf{p}_1|_{V_2=0}$. We can obtain $\mathbf{F}_{21}$ by exchanging the indices $1 \leftrightarrow 2$ in Eq. (38). The equation implies that $\mathbf{F}_{21} \neq -\mathbf{F}_{12}$ and thus violates Newton's third law. Such interactions have attracted a lot of attention recently and are often referred to as nonreciprocal.

Note that the leading-order interactions require both obstacles to be asymmetric so that $\mathbf{p}_k^0 \neq 0$. Nonetheless, when $O^{(2)}$ is symmetric, it still experiences a force from an asymmetric $O^{(1)}$ because the latter induces a density gradient in the vicinity of $O^{(2)}$ (Baek *et al.*, 2018). Finally, we note that, while two isotropic obstacles experience only short-range interactions, long-range interactions can also emerge even if all $\mathbf{p}_k^0$ vanish. For example, rods generate density modulations at order r_{12}^{-d} (Baek *et al.*, 2018).

We have considered dilute active fluids, but these derivations extend to the case of active bath particles subject to pairwise interactions (Granek *et al.*, 2020). Furthermore, a similar expansion has been derived for the interaction torque $\mathbf{n}_{12}$ between the obstacles (Baek *et al.*, 2018). The results also extend to multiple obstacles, yielding additive interactions to leading order in the far field.

D. Mobile obstacles and dynamics

Thus far we have discussed the case in which obstacles are fixed in space. However, there is also considerable interest in the dynamics of mobile obstacles, referred to as passive tracers in active baths. While a body of work focused on the effect of long-range hydrodynamic interactions in wet active baths [see, for example, Chen *et al.* (2007), Leptos *et al.* (2009), Kurtuldu *et al.* (2011), Zaid, Dunkel, and Yeomans (2011), Thiffeault (2015), Kurihara *et al.* (2017), and Kanazawa *et al.* (2020)], here we focus on dry scalar active matter with at most short-range interactions.

To write the emerging equations of motion of a tracer, we invoke an adiabatic limit where the motion of the tracer is so slow that the statistics of the forces exerted by the bath are indistinguishable from those exerted on a fixed tracer. In the overdamped limit, the dynamics of the tracer can then be described using a generalized Langevin equation (Steffenoni, Kroy, and Falasco, 2016; Maes, 2020; Reichert, Granz, and Voigtmann, 2021; Reichert and Voigtmann, 2021; Granek, Kafri, and Tailleur, 2022; Shea, Jung, and Schmid, 2022; Feng and Hou, 2023),

$$\int_0^t dt'\,\gamma_{ij}(t-t')\dot{X}_j(t') = f_i(t), \tag{39}$$

where $\gamma_{ij}(t)$ is a memory kernel, $f_i(t)$ is a fluctuating force, and summation over j is implied. The left-hand side of Eq. (39) is the friction force exerted by the bath, i.e., the average contribution to the force due to the motion of the tracer, while the right-hand side contains both the net force exerted on a fixed tracer and the fluctuations of the force exerted by bath particles. Unlike in equilibrium, $\langle\mathbf{f}(t)\rangle$ is generically nonzero for asymmetric tracers.

Within a systematic adiabatic expansion (D'Alessio, Kafri, and Polkovnikov, 2016), the memory kernel $\gamma_{ij}(t)$ is given by an Agarwal-Kubo-type formula

$$\gamma_{ij}(t) = \langle f_i(t)\partial_{X_j}\log P_{\mathrm{s}}(\{\mathbf{r}_k(0)-\mathbf{X},\mathbf{u}_k\})|_{\mathbf{X}=0}\rangle_c^{\mathrm{s}}, \tag{40}$$

where $\mathbf{r}_k$ and $\mathbf{u}_k$ are the positions and orientations of the bath particles, $P_{\mathrm{s}}(\{\mathbf{r}_k-\mathbf{X},\mathbf{u}_k\})$ is their many-body steady-state distribution, and $\langle\cdot\rangle^{\mathrm{s}}$ denotes an average with respect to an ensemble in which the tracer is held fixed. The subscript c indicates a connected correlation function, i.e., $\langle AB\rangle_c = \langle AB\rangle - \langle A\rangle\langle B\rangle$.

Likewise, the statistics of the fluctuating force $\mathbf{f}(t)$ are given by those of $\sum_k\boldsymbol{\nabla}V(\mathbf{r}_k-\mathbf{X})$ computed with the tracer held fixed, and where V is the interaction potential between the tracer and the active particles. For passive baths, the Boltzmann distribution $P_{\mathrm{s}}(\{\mathbf{r}_k-\mathbf{X},\mathbf{u}_k\}) \propto e^{-\beta\sum_k V(\mathbf{r}_k-\mathbf{X})}$ recovers from Eq. (40) the fluctuation-dissipation relation $\gamma_{ij}(t) = \beta\langle f_i(t)f_j(0)\rangle$. Out of equilibrium, this relation is generically broken, with interesting exceptions (Chun, Gao, and Horowitz, 2021; Han *et al.*, 2021).

1. Phenomenological description of symmetric tracers

For isotropic tracers, it is common to use a heuristic suggestion by Wu and Libchaber (2000) to describe their experiments on passive tracers; see also Fig. 12(a). They postulated $\gamma_{ij} = 2\Gamma_{\mathrm{T}}\delta(t-t')\delta_{ij}$ and $\langle f_i(t)f_j(0)\rangle_c = (D_{\mathrm{T}}\Gamma_{\mathrm{T}}^2 e^{-t/\tau_1}/\tau_1)\delta_{ij}$, with τ_1 a characteristic relaxation time and D_{T} a diffusion coefficient (Maggi *et al.*, 2017). Namely, the motion of the tracer behaves as an active particle with a mean-square displacement $\langle\mathbf{X}^2(t)\rangle_c$ given by

$$\langle\mathbf{X}^2(t)\rangle_c = 2dD_{\mathrm{T}}[t-\tau_1(1-e^{-t/\tau_1})]. \tag{41}$$

Equation (41) describes a crossover between a short-time ballistic motion ($\sim t^2$) and a long-time diffusive motion ($\sim t$) that is illustrated in Fig. 12(c). In the long-time limit, the particle diffuses as $\langle\mathbf{X}^2(t)\rangle_c \sim 2dD_{\mathrm{T}}t$.

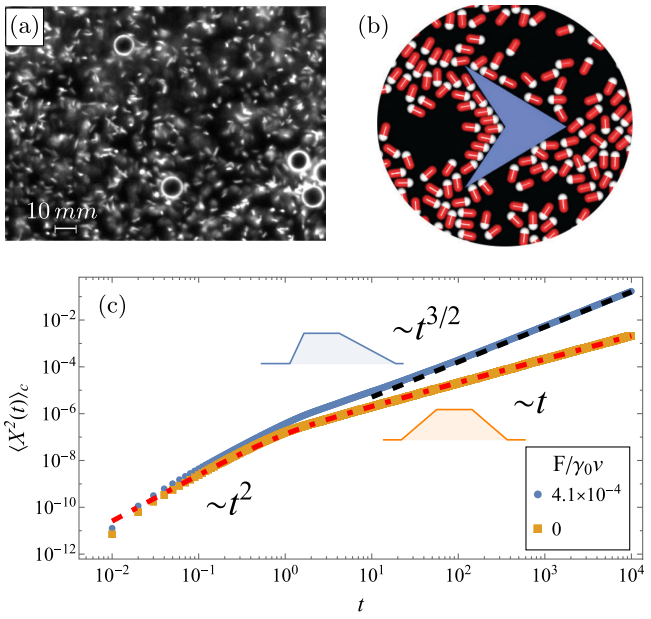

FIG. 12. (a) Passive polystyrene tracers immersed in a quasi-two-dimensional bacterial bath. Adapted from Wu and Libchaber, 2000. (b) Simulation snapshot of a V-shaped passive tracer in a two-dimensional active bath. Holding the tracer orientation fixed leads to an average directed motion to the right with velocity $\propto -\mathbf{p}$. From Angelani and Di Leonardo, 2010. (c) Mean-square displacement for an adiabatic passive tracer in a one-dimensional active bath (microscopic simulations). The symmetric tracer (the darker orange symbols) shows a transition from short-time ballistic to long-time diffusive motion. The dot-dashed red line depicts the Wu-Libchaber model [Eq. (41)], with the exact calculation of the diffusivity D_T from the adiabatic theory (see the text) and a fit leading to $\tau_1 = 0.41$. The asymmetric tracer (the lighter blue symbols) shows a long-time superdiffusion. The dashed black line represents the prediction [Eq. (48)] (no fitting parameters). All bath parameters are set to unity. From Granek, Kafri, and Tailleur, 2022.

2. The Markovian approximation

The long-time behavior can be obtained through more systematic methods, starting with microscopic models and using Taylor's dispersion theory (Burkholder and Brady, 2017, 2019; Peng and Brady, 2022) or singular perturbation methods (Solon and Horowitz, 2022; Jayaram and Speck, 2023). Assuming that γ_{ij} and $\langle f_i(t)f_j(0)\rangle_c$ decay exponentially in time, this leads to a Markovian approximation of Eq. (39) of the form

$$0 = -\Gamma_{ij}\dot{X}_j(t) + \xi_i(t). \tag{42}$$

In Eq. (42) $\boldsymbol{\xi}(t)$ is a Gaussian white noise that satisfies $\langle \xi_i(t)\xi_j(0)\rangle_c = 2I_{ij}\delta(t)$, while the friction coefficient Γ_{ij} and noise intensity I_{ij} are given by the Green-Kubo relations

$$\Gamma_{ij} = \int_0^\infty dt\, \gamma_{ij}(t), \tag{43}$$

$$I_{ij} = \int_0^\infty dt\, \langle f_i(t)f_j(0)\rangle_c^s. \tag{44}$$

This recovers the long-time diffusive behavior postulated by Wu and Libchaber.

Within the Markovian approximation and in the isotropic case where $I_{ij} = I\delta_{ij}$ and $\Gamma_{ij} = \Gamma_T\delta_{ij}$, one can identify an effective tracer temperature by $T_T = I/\Gamma_T = D_T\Gamma_T$. For hard-core tracers, the interpretation of T_T extends to an effective fluctuation-dissipation relation $\gamma_{ij}(t) \simeq T_T^{-1}\langle f_i(t)f_j(0)\rangle_c$ despite the system being out of equilibrium at the microscopic scale (Solon and Horowitz, 2022). We note, however, that, in contrast to equilibrium systems, the effective temperature depends on the properties of the tracer.

Note that, to model a tracer that is also in contact with a passive Markovian bath, one adds a thermostat $-\Gamma_{th}\dot{X}_i(t) + \sqrt{2\Gamma_{th}T_{th}}\eta_i(t)$ to Eqs. (39) and (42). The effective temperature then straightforwardly modifies to (Granek, Kafri, and Tailleur, 2022; Solon and Horowitz, 2022)

$$T_T = \frac{I + \Gamma_{th}T_{th}}{\Gamma_T + \Gamma_{th}} = \frac{\Gamma_T}{\Gamma_T + \Gamma_{th}}T_a + \frac{\Gamma_{th}}{\Gamma_T + \Gamma_{th}}T_{th}, \tag{45}$$

where $T_a \equiv I/\Gamma_T$ is the active contribution. Note that two different tracers put in the same bath generically experience two different temperatures, in contrast with the case of a passive bath.

The case of a soft tracer brings in interesting differences, as was recently shown in $d = 1$ (Granek, Kafri, and Tailleur, 2022). To begin, the fluctuation-dissipation relation survives only in the limit of a shallow wide tracer, for which the system converges to an equilibrium distribution $\rho(\mathbf{r}) \propto e^{-V(\mathbf{r})/T_{eff}}$ such that $T_a = T_{eff} = D_{eff}/\mu$. For small tracers, the local structure of the active bath around the tracer may enhance its motion and lead to an effective *negative friction coefficient* Γ_T (Granek, Kafri, and Tailleur, 2022). Microscopic simulations and a self-consistent calculation of the nonlinear tracer response reveal that the negative friction induces a spontaneous symmetry breaking and a nonzero average velocity in the limit $\rho_b \to \infty$ (Kim, Choe, and Baek, 2023). We note that, for hard tracers in $d > 1$, a related effect [called swim thinning (Burkholder and Brady, 2019)] was reported. The friction experienced by the tracer is reduced by the active bath (Burkholder and Brady, 2019; Knežević, Avilés Podgurski, and Stark, 2021; Peng and Brady, 2022; Jayaram and Speck, 2023), but negative frictions have not yet been reported in this case. The emergence of a negative friction out of equilibrium has recently attracted interest. For instance, in addition to the previously discussed case of a passive tracer in an active bath, a negative friction is also observed in the converse case, where an active tracer is pulled through a passive bath (Rizkallah *et al.*, 2023).

3. Beyond the Markovian approximation

It is well known that some care has to be taken when using a Markovian description to describe the long-time behavior of passive tracers. In particular, conservation laws lead to power-law decaying time correlation functions, which might cause the integrals [Eqs. (43) and (44)] to diverge (van Beijeren, 1982). For dry scalar active systems, the conserved density $\rho(\mathbf{r}, t)$ is diffusive and gives rise to slow hydrodynamic relaxation modes. For a system of size $L \gg \ell_p$, the relaxation

time grows as $\sim L^2$. For an infinite system and a fully symmetric tracer, the long-time tails of the force autocorrelation function and of γ_{ij} have been derived and shown to decay as $\sim t^{-(d/2+1)}$ (Granek, Kafri, and Tailleur, 2022; Solon and Horowitz, 2022; Feng and Hou, 2023), which is identical to the case of a tracer in a passive diffusive bath (Spohn, 1980; Hanna, Hess, and Klein, 1981; van Beijeren, 1982). The Green-Kubo integrals in Eqs. (43) and (44) then converge in any dimension, and the long-time diffusive behavior is unaffected.

Real tracers, however, always carry some degree of asymmetry, which leads to much different behaviors. The underlying reason is that the fluctuating force $\mathbf{f}(t)$ is nonzero on average, as discussed in Sec. IV.A. Indeed, in the adiabatic limit $\langle \mathbf{f}(t) \rangle = -\mathbf{p}$, which endows the tracer with an effective self-propulsion. Such dynamical rectification of random motion was first observed numerically by Angelani and Di Leonardo (2010) [see Fig. 12(b)] and later observed experimentally [in a wet system] (Kaiser *et al.*, 2014). Recently progress has been made in modeling the motion of asymmetric tracers (Knežević and Stark, 2020; Granek, Kafri, and Tailleur, 2022).

The asymmetric tracer's dynamics has been derived from first principles in $d = 1$ (Granek, Kafri, and Tailleur, 2022), where Eq. (39) continues to hold within an adiabatic expansion. Contrary to the case of the symmetric tracer, where the long-time tails $\sim t^{-3/2}$ lead to finite Green-Kubo integrals and effective long-time diffusion, the asymmetry shifts the decay to (Granek, Kafri, and Tailleur, 2022; Granek, 2023)

$$\langle f(t)f(0)\rangle_c = \frac{p^2}{\rho_b (4\pi D_{\mathrm{eff}} t)^{1/2}} + \mathcal{O}(t^{-3/2}), \tag{46}$$

$$\gamma(t) = \beta_{\mathrm{eff}} \langle f(t)f(0)\rangle_c + \mathcal{O}(t^{-3/2}), \tag{47}$$

rendering the Green-Kubo integrals infinite in $d = 1$. As long as the adiabatic approximation holds, one then predicts a superdiffusive behavior with

$$\langle X^2(t)\rangle_c \sim \frac{4p^2}{3\rho_b \Gamma_{\mathrm{th}}^2 \sqrt{\pi D_{\mathrm{eff}}}} t^{3/2}, \tag{48}$$

which is illustrated in Fig. 12(c). Likewise, the divergence in Eq. (43) is manifested in an apparent growth of the friction coefficient, measured from the average force required to tow the tracer at a constant velocity, as

$$\Gamma(t) \sim \frac{\mu p^2}{\rho_b D_{\mathrm{eff}}} \left(\frac{t}{\pi D_{\mathrm{eff}}}\right)^{1/2}. \tag{49}$$

These anomalous properties demonstrate that ratchet effects may induce a shift in the dynamical exponents caused by hydrodynamic modes.

Despite the theoretical advancement in the understanding of passive tracer dynamics, various questions remain open. For instance, the long-time tails in Eqs. (46) and (47) are expected to yield logarithmic corrections to the diffusion of an asymmetric tracer in $d = 2$, a phenomenon that is yet to be confirmed. Most importantly, exploring the dynamics in a controlled setting beyond the adiabatic limit remains an outstanding technical challenge.

E. Coupled dynamics of passive tracers: Nonreciprocal interactions and localization

When several mobile tracers are embedded in an active bath, their long-range interactions, described in Sec. IV.C, lead to interesting dynamical effects. Here we show how the nonreciprocal interactions between the tracers lead to phase transitions and how the interaction between a tracer and its boundary-induced image leads to a localization transition.

Consider pinned asymmetric objects, each free to rotate along a fixed axis; see Fig. 11. The density and current modulations induced by the obstacles generate torques on each other, leading to a Kuramoto-like dynamics of their orientations (Baek *et al.*, 2018). Analysis of this dynamics has shown a transition between a phase where the obstacles' orientations are locked and one in which they rotate in synchrony. While for the two-obstacle case studied by Baek *et al.* (2018) one observes a smooth crossover between these regimes, the many-body generalization studied by Fruchart *et al.* (2021) leads to bona fide phase transitions; see Fig. 13(a). Unpinning the two rotors was also shown to generate traveling bound states (Baek *et al.*, 2018). Similar bound states were subsequently found for active particles in passive mass-conserving baths (Dolai, Krekels, and Maes, 2022). It remains an interesting open question whether the many-body generalization of such states can lead to flocking or antiflocking, as was predicted via a nonreciprocal Vicsek model (Fruchart *et al.*, 2021) and a nonreciprocal active Ising model (Martin *et al.*, 2023).

Another interesting consequence of the nonreciprocal mediated interaction can be observed for a single asymmetric tracer in a spherical cavity; see Figs. 13(b) and 13(c). In this case, the generalized method of images described in Sec. IV.B determines the density and current modulations as the sum of contributions from the original tracer and its image upon a spherical inversion (Ben Dor, Kafri *et al.*, 2022). The nonreciprocal interactions between the object and its image lead to a transition from a steady-state distribution localized at the cavity wall to a distribution localized at its center. We stress that such a phenomenon is yet another signature of how different passive and active fluids are. In a dilute passive diffusive fluid, an object cannot experience any net force in a homogeneous system. To linear order, the sole force $\mathbf{f}$ it can experience is indeed proportional to $\boldsymbol{\nabla}\rho$. Consequently, in the steady state $\boldsymbol{\nabla} \cdot \mathbf{f} \propto \boldsymbol{\nabla}^2 \rho = 0$ since the fluid is diffusive. In analogy with Earnshaw's theorem in electrostatics, this rules out the possibility of a stable equilibrium for an object immersed in a passive diffusive fluid (Rohwer, Kardar, and Krüger, 2020; Ben Dor, Kafri *et al.*, 2022). Again, activity thus leads to a completely different physics.

F. Summary

In this section, we discussed the far-field density and current modulations induced by asymmetric obstacles and inclusions in scalar active fluids. This behavior is markedly different from that of equilibrium systems, where the

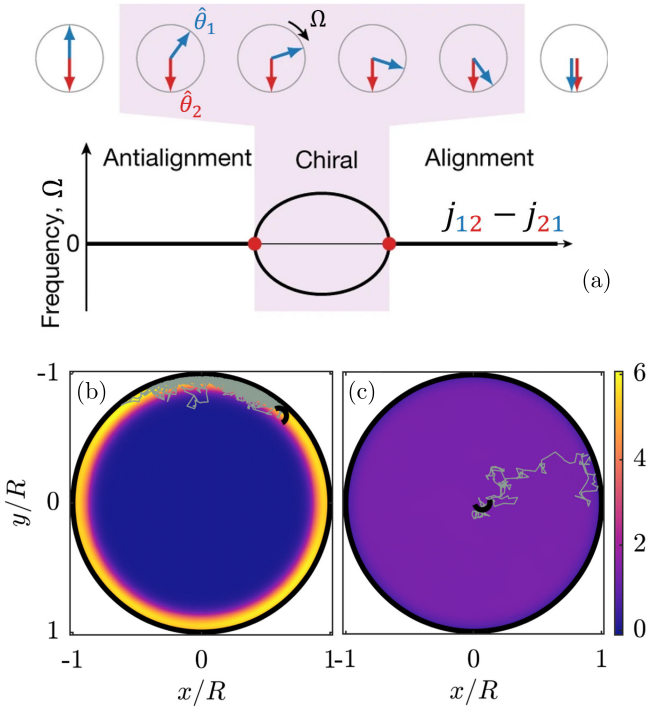

FIG. 13. (a) Nonreciprocal phase transitions. The nonreciprocal torque $\mathbf{n}_{12} = n_{12}\hat{\mathbf{z}}$ leads to an effective Kuramoto coupling $j_{12}\epsilon_{12} \propto n_{12}$, where ϵ_{ij} is the Levi-Civita symbol. The coupling asymmetry $j_{12} - j_{21}$ determines the steady-state frequency Ω and relative phase of $N \gg 1$ identical copies of rotors 1 and 2. When $\Omega \neq 0$, parity-time symmetry is spontaneously broken. From Fruchart *et al.*, 2021. (b),(c) Localization transition of an asymmetric obstacle in a spherical cavity. The probability density and typical trajectories of a passive tracer in the active bath are displayed. The rotational friction is set to (b) $\Gamma_r = 10^{-2}$ and (c) $\Gamma_r = 10^{-5}$. The particle speed is $v = 10^{-2}$. All other parameters are set to unity. From Ben Dor, Kafri *et al.*, 2022.

disturbances decay exponentially beyond the correlation length. Indeed, the power-law decay of density and current modulations reported for scalar active fluids lead to a rich dynamics of tracer particles and mobile obstacles. In particular, we discussed the emergence of nonreciprocal interactions between inclusions inserted in passive fluids and the phase transitions that they may generate.

V. BULK DISORDER

As discussed in Sec. IV, localized obstacles have a far-reaching impact on the properties of active fluids. When organized coherently, they can, for instance, act as pumps and generate large-scale flows or density gradients; see Fig. 10. This raises the question as to whether disordered assemblies of obstacles can also impact the properties of active fluids. In this Colloquium, we discuss the case of a quenched potential disorder, which corresponds to the evolution of a system under a fixed realization of a random potential. Experimentally, disorder is expected to be relevant in a range of situations: bacteria swim in soft disordered agar gel (Berg, 2004) or in a porous medium (Bhattacharjee and Datta, 2019), while active colloids (Howse *et al.*, 2007; Bricard *et al.*, 2013; Nishiguchi and Sano, 2015) or vibrated grains (Narayan, Ramaswamy, and Menon, 2007; Deseigne, Dauchot, and Chaté, 2010) can be placed next to rough surfaces.

For equilibrium systems, this question has attracted considerable interest, and many studies have been dedicated to the static and dynamical properties of passive systems in the presence of random potentials (Aharony, Imry, and Ma, 1976; Belanger *et al.*, 1983; Fisher, Fröhlich, and Spencer, 1984; Imbrie, 1984, 1985; Glaus, 1986; Bricmont and Kupiainen, 1987). We first review the results obtained in the passive case before turning to recent work on disordered scalar active matter. To characterize the impact of disorder on a scalar system, it is natural to consider density-density correlations, which are encoded in the structure factor. In experiments, the structure factor can be measured using scattering probes. For a system defined on a lattice of N sites, the structure factor is computed as

$$\overline{S(\mathbf{q})} \equiv \frac{1}{N}\sum_{\mathbf{r}} \overline{\langle \phi(\mathbf{r})\phi(0)\rangle}\, e^{i\mathbf{q}\cdot\mathbf{r}}, \tag{50}$$

where $\phi(\mathbf{r}) \equiv \rho(\mathbf{r}) - \rho_0$ measures the density fluctuations, the brackets stand for steady-state averages in a particular realization of disorder, and the overline represents an average over disorder realizations. In the "high-temperature" homogeneous phase, the impact of disorder can be computed using a Landau-Ginzburg field theory, which leads to the addition of a squared-Lorentzian form to the result in the absence of disorder (Glaus, 1986; Kardar, 2007),

$$\overline{S(\mathbf{q})} \propto \frac{1}{(\mathbf{q}^2 + \ell_c^{-2})^2}, \tag{51}$$

where ℓ_c is the correlation length of the density field. A natural question is then whether impurities can impact the existence of the ordered state and the nature of the phase transition. The first question was addressed some 50 years ago by Imry and Ma (1975), who showed that the lower critical dimension below which the system does not admit an ordered phase is $d_c = 2$. Moreover, Aizenman and Wehr (1989) showed that the system is also disordered at the marginal dimension of $d = 2$. This is illustrated in Figs. 14(a) and 14(b), where the ordered phase is destroyed by impurities and exhibits short-range correlations.

The active case is markedly distinct: In the homogeneous phase, the disorder leads to a scale-free steady state with a structure factor that diverges as (Ro *et al.*, 2021)

$$\overline{S(\mathbf{q})} \underset{q\to 0}{\propto} \frac{1}{\mathbf{q}^2}. \tag{52}$$

As shown in Fig. 15, fluctuations at small q are strongly enhanced compared to the passive case: The correlation length is infinite and density-density correlations decay as $\overline{\langle \phi(\mathbf{r})\phi(0)\rangle} \propto r^{2-d}$ for $d > 2$ and decay logarithmically in $d = 2$.

Beyond creating a long-range correlated fluid, disorder also has a strong impact on the existence of a long-range ordered phase. For a system undergoing MIPS, disorder prevents

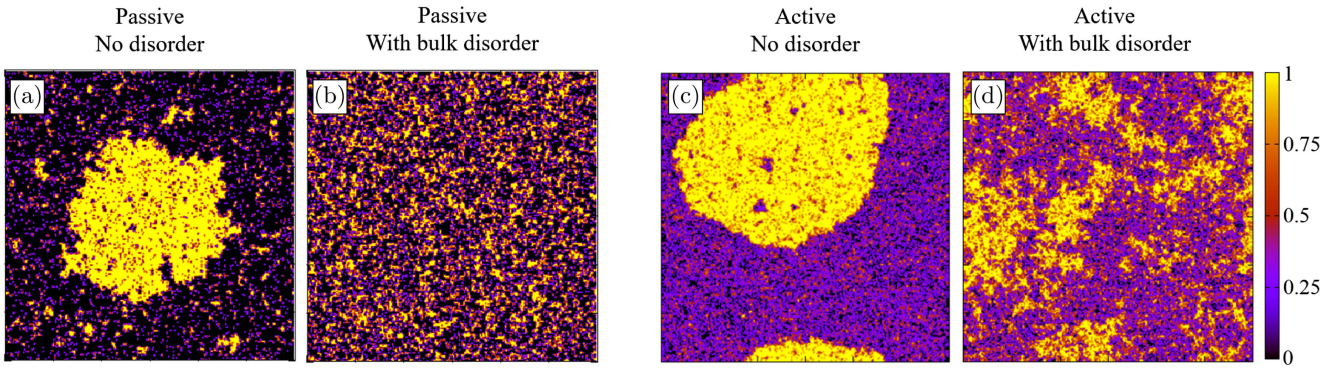

FIG. 14. Comparison between equilibrium and active systems undergoing phase separation. (a) A passive lattice gas with attractive interaction and (c) an active lattice gas with repulsive interactions may both experience bulk phase separation. (b) When a random potential is added to the passive system, the phase separation is suppressed, leading to a homogeneous phase with short-range correlations. (d) In the active case, a scale-free distribution of particles replaces the bulk phase separation. Color encodes density. From Ro *et al.*, 2021.

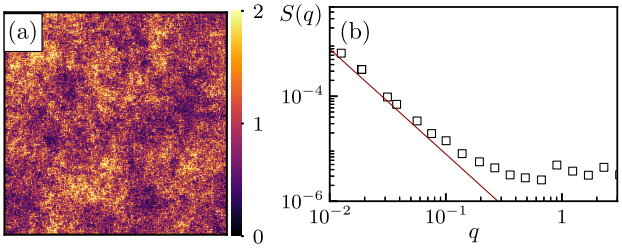

FIG. 15. Noninteracting active particles in the presence of a disordered potential. (a) Snapshot of the density field normalized by its average value $\rho(\mathbf{r})/\rho_0$. (b) Structure factor (symbols) compared to q^{-2} (red line), as predicted in Eq. (52). The results are obtained with RTPs on lattices with $v = 4$ and $\alpha = 1$, and the disorder potential is constructed by filling the space with square ramps with the size $\ell = 5$ and the height $\Delta V = 3.8$ in random locations and orientations.

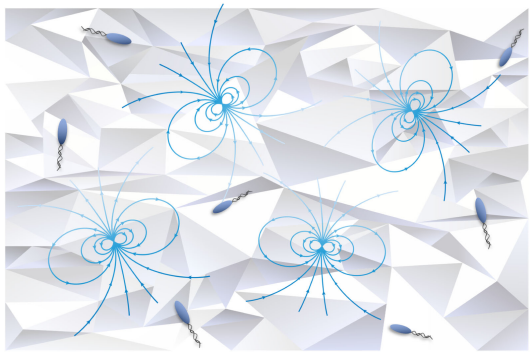

FIG. 16. Schematic depiction of disorder acting as a random array of pumps for active particles leading to a dipolar flow field.

phase separation in both two and three dimensions. Compared to the passive case, the lower critical dimension is increased from $d_c = 2$ to $d_c = 4$. As shown in Figs. 14(c) and 14(d), the phase-separated state is replaced by a frozen scale-free distribution with large-amplitude density fluctuations.

A. A simple physical picture

To understand the difference between the active and passive cases, we first recall the results of Sec. IV. At the microscopic scale, a random potential is generically asymmetric and thus, acting as a pump, it generates a ratchet current. As we now argue, the net effect of a dilute collection of randomly placed pumps is to generate density-density fluctuations consistent with Eq. (52), as depicted in Fig. 16.

To see this explicitly, consider a dilute distribution of pumps whose force density we denote by $\mathbf{f}(\mathbf{r})$. Each pump acts as a current source that modifies the density according to Eq. (32). The contributions from the pumps add up independently, resulting in the overall density modulation given by

$$\langle \phi(\mathbf{r}) \rangle = \beta_{\text{eff}} \int d^d\mathbf{r}' \, \mathbf{f}(\mathbf{r}') \cdot \boldsymbol{\nabla}_{\mathbf{r}} G(\mathbf{r} - \mathbf{r}'), \tag{53}$$

where $G(\mathbf{r} - \mathbf{r}') = G(\mathbf{r}, \mathbf{r}')$ is the Green's function of the Laplacian. Note that for a single pump $\mathbf{f}(\mathbf{r}) = \mathbf{p}\delta^d(\mathbf{r} - \mathbf{r}_0)$, Eq. (53) returns the solution Eq. (30) derived in Sec. IV.A for an isolated asymmetric inclusion. In Fourier space, the convolution in Eq. (53) takes the form[5]

$$\langle \phi(\mathbf{q}) \rangle = \beta_{\text{eff}} L^{d/2} i\mathbf{q} \cdot \mathbf{f}(\mathbf{q}) G(\mathbf{q}),$$

where $G(\mathbf{q}) = -L^{-d/2} q^{-2}$, $q = |\mathbf{q}|$, and L is the system size. Assuming Gaussian-distributed uncorrelated pumps with a typical strength χ, $\mathbf{f}(\mathbf{q})$ is entirely characterized by

$$\overline{f_i(\mathbf{q})} = 0,$$
$$\overline{f_i(\mathbf{q}) f_j(\mathbf{q}')} = \chi^2 \delta_{ij} \delta_{\mathbf{q},-\mathbf{q}'}.$$

For noninteracting particles, the structure factor satisfies $\overline{\langle \phi(\mathbf{q}) \phi(-\mathbf{q}) \rangle} = \overline{\langle \phi(\mathbf{q}) \rangle \langle \phi(-\mathbf{q}) \rangle}$ such that

[5]In what follows we use the Fourier convention $f(\mathbf{q}) = L^{-d/2} \int d^d\mathbf{r} \, e^{-i\mathbf{q}\cdot\mathbf{r}} f(\mathbf{r})$ and $f(\mathbf{r}) = L^{-d/2} \sum_{\mathbf{q}} e^{i\mathbf{q}\cdot\mathbf{r}} f(\mathbf{q})$.

$$\overline{\langle\phi(\mathbf{q})\phi(-\mathbf{q})\rangle} = \frac{\beta_{\mathrm{eff}}^2}{q^4}\sum_{i,j=1}^{d} q_i q_j \overline{f_i(\mathbf{q})f_j(-\mathbf{q})} = \frac{\beta_{\mathrm{eff}}^2\chi^2}{q^2}, \tag{54}$$

which is indeed compatible with the 2D structure factor presented in Fig. 15.

B. Field-theoretical description

To account for the effects of interactions between the particles, it is useful to introduce a field-theoretical description by building upon the insights of the previous section. Since the quenched random potential translates, through the ratchet effect, into a quenched random forcing, one can start with a simple linear field theory of the form

$$\frac{\partial}{\partial t}\phi(\mathbf{r},t) = -\boldsymbol{\nabla}\cdot\mathbf{j}(\mathbf{r},t), \tag{55}$$

$$\mathbf{j}(\mathbf{r},t) = -\boldsymbol{\nabla}\mathfrak{u}[\phi] + \mathbf{f}(\mathbf{r}) + \sqrt{2D}\boldsymbol{\eta}(\mathbf{r},t), \tag{56}$$

where $\phi(\mathbf{r},t)$ describes the coarse-grained density fluctuations, $\mathbf{j}(\mathbf{r},t)$ is the associated current, and $\boldsymbol{\eta}(\mathbf{r},t)$ is a centered Gaussian white noise field such that $\langle\eta_i(\mathbf{r},t)\eta_j(\mathbf{r}',t')\rangle = \delta_{ij}\delta(t-t')\delta(\mathbf{r}-\mathbf{r}')$. The mobility is set to 1 and, as in the previous section, the force density satisfies $\overline{f_i(\mathbf{r})} = 0$ and $\overline{f_i(\mathbf{r})f_j(\mathbf{r}')} = \sigma^2\delta_{ij}\delta^d(\mathbf{r}-\mathbf{r}')$. At a linear level in ϕ and to leading order in a gradient expansion, the effective chemical potential $\mathfrak{u}$ is of the form

$$\mathfrak{u}[\phi(\mathbf{r},t)] = u\phi(\mathbf{r},t) - K\boldsymbol{\nabla}^2\phi(\mathbf{r},t), \tag{57}$$

with $u, K > 0$ to ensure stability.

Before proceeding, we highlight the difference between the current induced by the force density $\mathbf{f}(\mathbf{r})$ and the Brownian noise $\boldsymbol{\eta}(\mathbf{r},t)$. To do so, we consider the time-averaged total current, denoted as

$$\boldsymbol{J} = \frac{1}{\Delta t}\int_0^{\Delta t} dt \int d^d\mathbf{r}\,\mathbf{j}(\mathbf{r},t), \tag{58}$$

flowing through the entire system during the time interval Δt in the presence of disorder and periodic boundary conditions. The magnitude of $\boldsymbol{J}$ can be characterized by averaging $\mathcal{J}^2$ over both noise and disorder. Direct algebra shows that this second moment is given by

$$\overline{\langle\mathcal{J}^2\rangle} = d\sigma^2 L^d + 2dDL^d\Delta t^{-1}. \tag{59}$$

Equation (59) demonstrates that, although the scaling with the system size is the same for both the random force and noise-induced terms, the scaling with the time interval is drastically different. The quenched random force induces a net stationary current, which remains finite as $\Delta t \to \infty$. By contrast, the current fluctuations induced by the Brownian noise decay as Δt^{-1} once averaged over the time interval Δt. To verify this prediction, we measure $\boldsymbol{J}$ by simulating RTPs with and without disorder, subject to periodic boundary conditions. The scaling of the second moment with the system size shown in Fig. 17(a) indeed confirms Eq. (59). In Fig. 17(b), we show how the second moment scales with the observation time interval, both with and without disorder. In the absence of disorder, $\boldsymbol{J}$ is dominated by the time-dependent noise, and its second moment indeed shows a diffusive scaling $\overline{\langle\mathcal{J}^2\rangle} \propto \Delta t^{-1}$ (the red symbols). In the presence of disorder, the ballistic contribution of the random force dominates the long-time scaling, as confirmed by our simulation (the blue symbols).

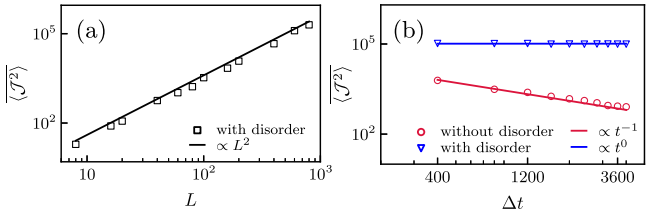

FIG. 17. Scaling of the time-averaged total current with respect to (a) the system size and (b) the measurement time interval. The second moment $\overline{\langle\mathcal{J}^2\rangle}$ measured in simulation (symbols) is compared to the scaling trends predicted in Eq. (59) (solid lines). The parameters are $d = 2$, particle speed $v = 4$, the amplitude of the random potential $\Delta V = 3.8$, $\Delta t = 4000$ in (a), $L = 800$ in (b), and averaged over 50 realizations of disorder.

We now turn to the discussion of the density-density correlations. A direct computation using Eqs. (55)–(57) shows that the structure factor of the linearized theory is given by

$$S(\mathbf{q}) = \frac{\sigma^2}{q^2(u+Kq^2)^2} + \frac{D}{(u+Kq^2)}. \tag{60}$$

We note that Eqs. (60) and (54) predict the same small-q behavior upon identifying σ/u with $\chi\beta_{\mathrm{eff}}$. To check the relevance of nonlinearities, terms of the form $s\phi^n(\mathbf{r},t)$ can be added to the effective chemical potential $\mathfrak{u}$, and their relevance can be accessed under diffusive scaling $\mathbf{r} \to b\mathbf{r}$ and $t \to b^2 t$ in Eqs. (55) and (56). Since the structure factor satisfies $\overline{\phi(\mathbf{q})\phi(\mathbf{q}')} \propto q^{-2}\delta^d(\mathbf{q}+\mathbf{q}')$, the density modulations in real space are first rescaled as $\phi \to b^{1-d/2}\phi$. Accordingly, any nonlinear term transforms as $\phi^n \to b^{n(1-d/2)}\phi^n$, and they are irrelevant for $d > 2$. The case $d = 2$ is marginal, and Ro *et al.* (2021) showed that the theory is self-consistent up to length scales such that $\ell \ll \ell^*$ with $\ell^* \equiv a\exp(\pi u^2\rho_b^2/\sigma^2)$. Beyond such length scales, which have never been explored numerically, a different behavior for $S(\mathbf{q})$ may emerge.

We now discuss how a generalization of the Imry-Ma argument predicts the destruction of an ordered phase in dimensions below the lower critical dimension of $d_c = 4$. To begin, using a Helmholtz-Hodge decomposition, we write the random force field as[6]

$$\mathbf{f}(\mathbf{r}) = -\boldsymbol{\nabla}U(\mathbf{r}) + \boldsymbol{\Xi}(\mathbf{r}), \tag{61}$$

[6]In the reported simulations, periodic boundary conditions were employed and the Helmholtz-Hodge decomposition also includes harmonic functions that are linear combinations of constant flows along the system axes. They do not impact the discussion of the generalized Imry-Ma argument.

where $U(\mathbf{r})$ is an *effective potential* that differs from $V(\mathbf{r})$ and the vector field $\boldsymbol{\Xi}(\mathbf{r})$ satisfies $\boldsymbol{\nabla}\cdot\boldsymbol{\Xi}(\mathbf{r})=0$. We note that $\boldsymbol{\Xi}$ impacts the current but not the dynamics of the density field or its distribution. The statistics of $\mathbf{f}(\mathbf{r})$ imply that

$$\overline{U(\mathbf{q})U(\mathbf{q}')}=\sigma^2 q^{-2}\delta^d_{\mathbf{q},-\mathbf{q}'}, \tag{62}$$

$$\overline{\Xi_i(\mathbf{q})\Xi_j(\mathbf{q}')}=\sigma^2(\delta_{ij}-q_iq'_j/q^2)\delta^d_{\mathbf{q},-\mathbf{q}'}, \tag{63}$$

$$\overline{U(\mathbf{q})\boldsymbol{\Xi}(\mathbf{q}')}=0. \tag{64}$$

Because we are considering a linear theory and $\boldsymbol{\Xi}$ is divergence free, the dynamics of the density field is equivalent to an equilibrium dynamics in a potential $U(\mathbf{r})$ (Ao, 2004; Kwon, Ao, and Thouless, 2005). Inspection of Eq. (62) shows that $U(\mathbf{r})$ behaves like a Gaussian free field that is equivalent to a random surface in $d=2$. Its deep and scale-free minima account for the long-range correlations experienced by the density field. Furthermore, we can now predict the lower critical dimension by applying the standard Imry-Ma argument to an equilibrium dynamics in the presence of the potential $U(\mathbf{r})$ (Imry and Ma, 1975; Aharony, Imry, and Ma, 1976). This entails comparing the surface energy cost of overturning an ordered domain of linear size ℓ (given by $\gamma\ell^{d-1}$, with γ a surface-tension-like coefficient) to the bulk energy gain of the domain due to a locally favorable disorder potential. The latter, given by $E(\ell)=\int_{\ell^d}d^d\mathbf{r}'\rho_0U(\mathbf{r}')$, has a typical value of $E(\ell)\propto\sigma\rho_0\ell^{1+d/2}$ that is estimated by noting that the variance satisfies $\overline{E(\ell)^2}=\sigma^2\rho_0^2\ell^{d+2}$. For $d<4$, the surface energy cost is negligible on large enough length scales, and the system cannot phase separate into macroscopic domains.

We note that the field theory studied in Eqs. (53)–(56) is equivalent to that describing passive particles in a random force field. At the single-particle level, this system has attracted some attention in the past (Derrida and Pomeau, 1982; Derrida, 1983; Sinai, 1983; Fisher, 1984; Bouchaud *et al.*, 1990), and the previous analysis extends this work to the many-body case. We note that, for active particles in a random potential, the one-dimensional dynamics can be shown to be equivalent to a Sinai random walk (Ben Dor *et al.*, 2019). In higher dimensions, the dynamics remains to be studied.

VI. BOUNDARY DISORDER

In equilibrium, boundaries and boundary conditions generically do not alter bulk phase behaviors, due to the subextensive nature of their contributions to the free energy. This is illustrated in Fig. 18, where replacing flat confining walls with rough ones has no impact on bulk phase separation. An important consequence is that, in simulations or theoretical analysis, convenient boundary conditions (open or periodic) are often used to study bulk properties in equilibrium statistical mechanics.

Boundary disorder can be implemented by confining active particles using rough boundaries. This can be easily engineered for macroscopic vibrated grains by adapting the setup of Deseigne, Dauchot, and Chaté (2010). On the microscopic scale, rough walls can be engineered using microlithography and reactive ion etching by following Galajda *et al.* (2007). On the theoretical side, the disordered boundary can be modeled using a wall potential $V(x,\mathbf{r}_\parallel)$, where x is the coordinate normal to the wall and $\mathbf{r}_\parallel$ is a $(d-1)$-dimensional vector parallel to the wall. For example, $V(x,\mathbf{r}_\parallel)$ can be modeled by setting $V(x<0,\mathbf{r}_\parallel)=\infty$ and placing wedge-shaped asymmetric obstacles along the wall whose orientations are chosen randomly; see Figs. 18(b) and 19(b) for qualitative illustrations. The obstacles then have a finite extent x_w in the $\hat{\mathbf{x}}$ direction.

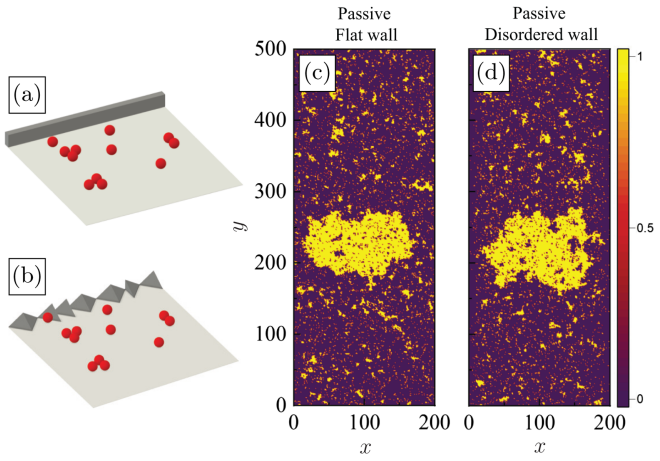

FIG. 18. The impact of (a) flat and (b) disordered walls on phase separation in passive systems. (c),(d) In the presence of attractive interactions between particles, simulations of a passive lattice gas at low temperature show phase separation in both settings. Color and brightness encode density. From Ben Dor, Ro *et al.*, 2022.

Figure 19 then shows a striking difference with the passive case: the rough "disordered" walls destroy bulk phase separation, leading to a nontrivial density distribution. This was shown to hold even in the macroscopic limit where the boundaries are sent to infinity. It shows that, even in the

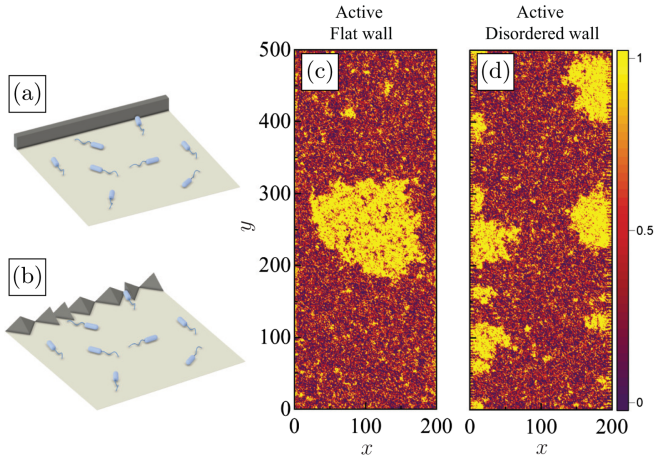

FIG. 19. Impact of (a) flat and (b) disordered walls on phase separation in active systems. In contrast to the passive case shown in Fig. 18, (d) simulations of an active lattice gas show that (c) the disordered boundary destroys the phase separation observed in the presence of a flat wall, leading to a scale-free distribution of particles. Color encodes density. From Ben Dor, Ro *et al.*, 2022.

thermodynamic limit, the bulk behaviors of active systems with closed or periodic boundary conditions can be markedly different (Ben Dor, Ro *et al.*, 2022), in stark contrast with passive systems (away from critical points). As we now discuss, the far-field density modulations and currents induced by such a disordered wall and their effects on the bulk behavior can be computed by modeling the disordered wall as a collection of force monopoles randomly placed at $x = 0$ and oriented along the $\mathbf{r}_\parallel$ surface.

A. A simple physical picture

Again we start by considering the dilute case and describe the force monopoles using a quenched Gaussian random force density $\mathbf{f}(\mathbf{r}_\parallel, x)$ whose statistics satisfy

$$\overline{f_i(\mathbf{r}_\parallel, x)} = 0,$$
$$\overline{f_i(\mathbf{r}_\parallel, x) f_j(\mathbf{r}'_\parallel, x')} = 2\chi^2 \delta^\parallel_{ij} \delta(x)\delta(x')\delta^{(d-1)}(\mathbf{r}_\parallel - \mathbf{r}'_\parallel), \quad (65)$$

where χ sets the scale of the force density, $\delta^\parallel_{ij} = 1$ if $i = j \neq x$ and $\delta^\parallel_{ij} = 0$ otherwise. As in the bulk disorder case, the density modulations in the system satisfy

$$\langle \phi(\mathbf{r}) \rangle = \beta_{\text{eff}} \int d^d\mathbf{r}' \, \mathbf{f}(\mathbf{r}') \cdot \boldsymbol{\nabla}_{\mathbf{r}} G_{\text{w}}(\mathbf{r}, \mathbf{r}'), \quad (66)$$

but this time $G_{\text{w}}(\mathbf{r}, \mathbf{r}')$ is the Green's function associated with a Poisson equation in a half-infinite system with Neumann boundary conditions at $x = 0$; see Sec. IV.B. Using this, one finds that the two-point correlation function satisfies (Ben Dor, Ro *et al.*, 2022)

$$\overline{\langle \phi(x, \mathbf{r}_\parallel)\phi(x', \mathbf{r}'_\parallel) \rangle} = \frac{2\beta_{\text{eff}}\chi(x + x')}{S_d[(x + x')^2 + |\Delta\mathbf{r}_\parallel|^2]^{d/2}}, \quad (67)$$

with S_d the d-dimensional solid angle and $\Delta\mathbf{r}_\parallel = \mathbf{r}_\parallel - \mathbf{r}'_\parallel$. Equation (67) shows that there are large-scale density modulations that decay in amplitude but increase in range as one looks further from the wall.

The heuristic prediction [Eq. (67)] is verified numerically in Fig. 20 using microscopic simulations of noninteracting particles in two space dimensions. To do so, the prediction Eq. (67) for $x = x'$ can be rewritten as

$$\frac{\overline{\langle \phi(x, y)\phi(x, y + \Delta y) \rangle}}{\overline{\langle \phi(x, y)\phi(x, y) \rangle}} = \frac{1}{1 + [\Delta y/(2x)]^2} \equiv \mathcal{S}\left(\frac{\Delta y}{x}\right), \quad (68)$$

which highlights that the correlations along y increase linearly with the distance x to the wall.

An illuminating way to understand these results is to consider the currents generated in the system: the ratchet mechanism generates local currents in the active fluid next to the wall. Since the number of particles is conserved, this microscopic stirring develops into large-scale eddies in the bulk. In fact, on large scales the current can be estimated as $\mathbf{J}(x, \mathbf{r}_\parallel) \approx -D_{\text{eff}} \boldsymbol{\nabla}\phi(x, \mathbf{r}_\parallel)$, which leads to

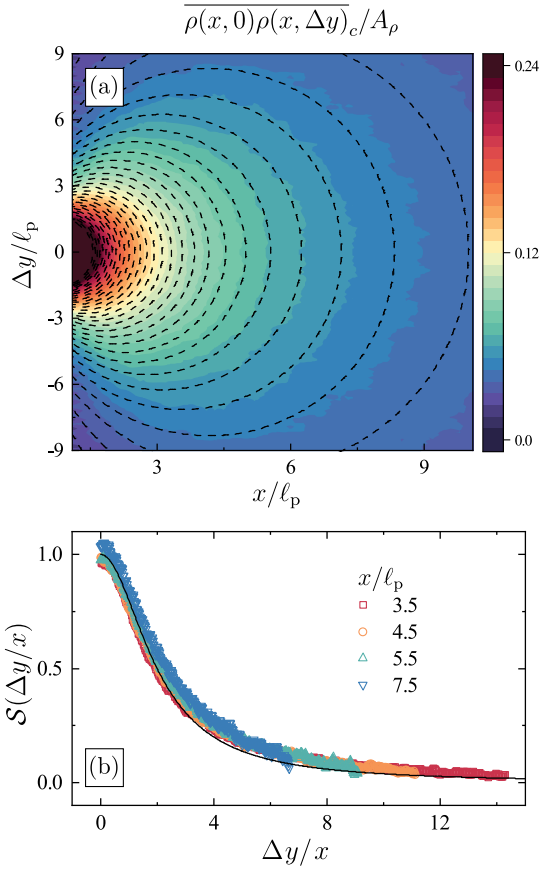

FIG. 20. Disorder-averaged two-point density correlation function of noninteracting RTPs in two dimensions in the presence of a disordered wall at $x = 0$. (a) The two-point correlation function as x and Δy are varied, calculated from simulations, is indicated by the color map (the darker color nearby the origin indicates large correlation). The value of $A_\rho \equiv \ell_{\text{p}} S_d^{-1} (2\beta_{\text{eff}}\chi)^2$ is obtained from a fit of the data to Eq. (67). The theoretical prediction of Eq. (67) is then used to produce dashed contour lines that match the levels of the color bar. Both theory and simulations are normalized by A_ρ. (b) A verification of the scaling form [Eq. (68)] for the density-density correlation function. The data shown in (a) for four different distances x from the wall are collapsed onto a single curve, as predicted. From Ben Dor, Ro *et al.*, 2022.

$$\overline{\langle \mathbf{J}(x, \mathbf{q}_\parallel) \cdot \mathbf{J}^*(x, \mathbf{k}_\parallel) \rangle}$$
$$= 2^d d(\mu\chi)^2 |\mathbf{q}_\parallel|^2 e^{-2|\mathbf{q}_\parallel|x} \times \pi^{d-1}\delta^{(d-1)}(\mathbf{q}_\parallel + \mathbf{k}_\parallel). \quad (69)$$

The current-current correlations first increase for small $|\mathbf{q}_\parallel|$ and then are exponentially suppressed for $|\mathbf{q}_\parallel| > x^{-1}$. Like the density-density correlations, the eddies have a transverse extent that grows linearly with the distance x to the wall, as verified in Fig. 21 using a scaling form similar to that of Eq. (68).

B. Linear field theory

To account for interactions, we follow Sec. V.B and use the linear field theory equations (55) and (56) to describe the evolution of the density fluctuations $\phi(\mathbf{r}, t)$. This time, however, the statistics of the random force field $\mathbf{f}(\mathbf{r})$ satisfy

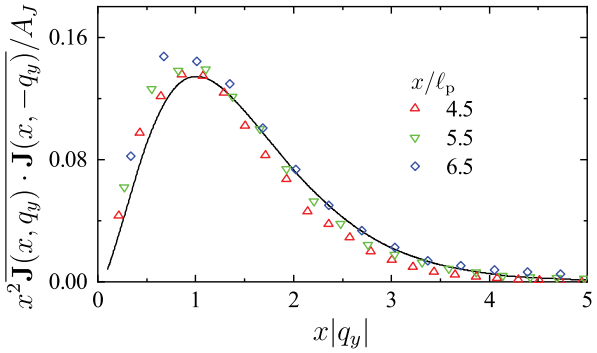

FIG. 21. Fourier transform along the $\hat{\mathbf{y}}$ direction of the current-current correlation function measured at a distance x from the wall and averaged over disorder. The data are obtained for three values of x and normalized by a factor $A_J \equiv 2d(2\pi)^{d-1}(\mu\chi)^2$. As predicted by the theory, the data can be collapsed onto a single curve corresponding to Eq. (69) by properly scaling the abscissa and the ordinates. From Ben Dor, Ro *et al.*, 2022.

$$f_x(x,\mathbf{r}_\parallel) = 0, \tag{70}$$

$$\overline{f_i(x,\mathbf{r}_\parallel)} = 0,$$
$$\overline{f_i(x,\mathbf{r}_\parallel)f_j(x',\mathbf{r}'_\parallel)} = 2\sigma^2\delta_{ij}\delta(x)\delta(x')\delta^{(d-1)}(\mathbf{r}_\parallel - \mathbf{r}'_\parallel), \tag{71}$$

where i and j label directions parallel to the wall. The amplitude σ of the random force density depends on the average bulk density ρ_b but is, to leading order, independent of ϕ. Direct algebra shows that this linear field theory predicts density modulations and currents compatible with the prediction [Eqs. (68) and (69)] on large length scales upon identifying $2\chi\beta_{\text{eff}} = \sigma/u$.

The self-consistency of the linear theory can be checked using a scaling argument similar to what was employed for the bulk disorder in Sec. V.B. This time, nonlinearities are found to be irrelevant for $d > 1$. We now discuss how the field theory allows the impact of boundary disorder on bulk phase separation in active fluids to be estimated.

C. The effect of disordered boundaries on MIPS

Again, one uses the Helmholtz-Hodge decomposition (61) of the random forcing to identify an effective potential $U(\mathbf{r})$. Since the effective potential satisfies $\boldsymbol{\nabla}^2 U(\mathbf{r}) = -\boldsymbol{\nabla}\cdot\mathbf{f}(\mathbf{r})$, Eqs. (70) and (71) imply that the statistics of U obey

$$\overline{U(\mathbf{r})} = 0, \tag{72}$$

$$\overline{U(\mathbf{r})U(\mathbf{r}')} = \frac{\sigma^2}{S_d}\frac{x+x'}{[(x+x')^2 + |\Delta\mathbf{r}_\parallel|^2]^{d/2}}. \tag{73}$$

This can then be used to compare the surface energy $\gamma\ell^{d-1}$ of an ordered droplet of linear size ℓ to its bulk energy $\int_{\ell^d} d^d\mathbf{r}U(\mathbf{r})$. Using Eq. (73), one can estimate the latter to scale as $\ell^{(d+1)/2}$ so that the surface energy is unable to stabilize a macroscopic droplet below a lower critical dimension $d_c = 3$. As shown in Fig. 19, the phase-separated state is indeed replaced by scale-free density modulations in $d = 2$. This result highlights how boundaries can play a much more important role in active systems than in their passive counterparts.

VII. CONCLUSION AND PERSPECTIVES

In this Colloquium, we have reviewed the anomalous mechanical properties of dry scalar active systems that have recently attracted significant attention. We have shown how the emergence of ratchet currents and the lack of conservation of momentum lead to a wide variety of phenomena, from the lack of an equation of state for pressure to the destruction of bulk phase separation by boundary disorder, all of which can be captured within a unifying perspective. These phenomena endow active systems with properties that are strikingly different from those of passive matter, whose consequences are only starting to be explored. Many open challenges now need to be addressed.

- While the physics of pressure starts to be well understood, *surface tension* remains an elusive concept in active-matter systems. Its definition remains under debate (Bialké *et al.*, 2015; Bettolo Marconi Marini, Maggi, and Melchionna, 2016; Paliwal *et al.*, 2017; Hermann, de las Heras, and Schmidt, 2019; Omar, Wang, and Brady, 2020; Fausti *et al.*, 2021; Lauersdorf *et al.*, 2021) to the extent that there is not even an agreement on the sign of the liquid-gas surface tension experienced by an interface in a system undergoing MIPS. Beyond the sole concept of surface tension, the entire question of wetting in active matter is largely uncharted territory (Sepúlveda and Soto, 2018; Pérez-González *et al.*, 2019; Turci, Wilding, and Jack, 2024; Zhao *et al.*, 2024).
- From a broader perspective, the fate of most *thermodynamic state functions* in active systems remains to be explored. We do not understand either the fate of, say, the chemical potential in active systems or what the new state functions are, if any, when there is no equation of state for pressure. This discussion is particularly relevant when one tries to put active matter to work, say, to build *active engines*. This is a topic that has attracted substantial interest lately, at both the theoretical (Zakine *et al.*, 2017; Pietzonka *et al.*, 2019; Ekeh, Cates, and Fodor, 2020; Holubec and Marathe, 2020; Fodor and Cates, 2021; Datta, Pietzonka, and Barato, 2022; Speck, 2022b) and experimental levels (Di Leonardo *et al.*, 2010; Sokolov *et al.*, 2010; Maggi, Saglimbeni *et al.*, 2015).
- Beyond the desire to extract work from active-matter systems, the question of their control has also attracted significant attention. This is true at the macroscopic scale, with the challenging issues involved in controlling drone and robot swarms (Vásárhelyi *et al.*, 2018; Ben Zion *et al.*, 2023), but also at the microscopic one, where active particles have been suggested as a possible way to implement targeted delivery at the micrometer scale (Koumakis *et al.*, 2013).

- All the phenomena discussed in this Colloquium are addressed in the limit where boundaries and inclusions are either immobile or move on timescales much longer than the relaxation time of the active bath. The response of active systems to time-dependent perturbations, however, has been only lightly studied (Sándor *et al.*, 2017; Frangipane *et al.*, 2018; Maggi *et al.*, 2018; Rohwer *et al.*, 2018; Rohwer, Kardar, and Krüger, 2020).
- Furthermore, in this Colloquium we have focused on dry scalar active matter to single out the interesting phenomena that are due solely to the interplay between activity and mechanical forces. Other situations, where more hydrodynamic fields are relevant, are bound to lead to an even richer physics. In particular, the role of obstacles, boundaries, and disorder in wet active matter is a current frontier in the field (Lauga and Powers, 2009; Takagi *et al.*, 2014; Sipos *et al.*, 2015; Spagnolie *et al.*, 2015; Elgeti and Gompper, 2016; Creppy *et al.*, 2019; Maitra, 2023; de Pirey, Kafri, and Ramaswamy, 2024). Given the rich behaviors already observed in scalar active systems, it is also natural to expect aligning active matter to lead to an even richer physics. The responses of polar systems to perturbations (Codina *et al.*, 2022), fluctuations (Benvegnen *et al.*, 2023), and disorder (Peruani and Aranson, 2018; Toner, Guttenberg, and Tu, 2018b; Chardac *et al.*, 2021; Duan *et al.*, 2021) have indeed attracted substantial attention, but our understanding of this case is much less advanced than in the simpler setting discussed in this Colloquium.

Finally, much of the research thus far has been based on theoretical studies of minimal models. Beyond the previously discussed questions, how the anomalous mechanical properties can be measured or harnessed in experimental active-matter systems is an interesting research direction (Junot *et al.*, 2017). Similarly, the far-field density and current modulations induced by localized obstacles, as well as the scale-free state induced by bulk and boundary disorder, are within reach of modern experimental active-matter systems (Bhattacharjee and Datta, 2019; Chardac *et al.*, 2021; Takaha and Nishiguchi, 2023). Their measurement is an ongoing challenge.

ACKNOWLEDGMENTS

This Colloquium was born out of many discussions and collaborations on the mechanical properties of scalar active systems that have involved many colleagues. In particular, we are grateful to Yongjoo Baek, Aparna Baskaran, Ydan Ben Dor, Mike Cates, Adrian Daerr, Yaouen Fily, Jordan Horowitz, Nikolai Nikola, Gianmarco Spera, Joakim Stenhammar, Ari Turner, Frédéric van Wijland, Raphaël Voituriez, Ruben Zakine, and Yongfeng Zhao. We also thank Ram Adar for a critical reading of the manuscript. J. T. thanks ANR THEMA for the financial support and MSC Laboratory for the hospitality. M. K. is supported by NSF Grant No. DMR-2218849. Y. K., O. G., and S. R. acknowledge financial support from ISF (Grant No. 2038/21) and NSF/BSF (Grant No. 2022605). O. G. also acknowledges support from the Adams Fellowship Program of the Israel Academy of Science and Humanities.

APPENDIX: MOTILITY-INDUCED PHASE SEPARATION

In this appendix, we provide an overview of the hydrodynamic description of MIPS in Sec. A.1, which legitimates the linear field theory employed in Secs. V and VI. We discuss in Sec. A.2 the richer physics encountered in a variety of MIPS-related phenomena. The impact of bulk and boundary disorders in such systems remains uncharted territory.

1. A minimal hydrodynamic description of MIPS

MIPS was first observed in collections of RTPs interacting via quorum sensing, which belong to the class of quorum-sensing active particles (QSAPs) [see Fig. 22(a)] whose self-propulsion speed $v_p = \mu f_p$ decreases rapidly enough as the local density increases (Tailleur and Cates, 2008). For this system, it is possible to derive a fluctuating hydrodynamics for the density field as

$$\partial_t \hat{\rho} = \boldsymbol{\nabla} \cdot [\hat{\rho} \mathcal{D}_{\mathrm{eff}} \boldsymbol{\nabla} \mathbf{u} + \sqrt{2\hat{\rho}\mathcal{D}_{\mathrm{eff}}}\boldsymbol{\Lambda}]. \tag{A1}$$

In Eq. (A1), the density field is constructed from the N particle positions as

$$\hat{\rho}(\mathbf{r}, t) \equiv \sum_{i=1}^{N} \delta[\mathbf{r} - \mathbf{r}_i(t)], \tag{A2}$$

$\mathcal{D}_{\mathrm{eff}}(\mathbf{r}, [\hat{\rho}]) = v^2(\mathbf{r}, [\hat{\rho}])\tau/d$ is the large-scale diffusivity, $\mathbf{u}(\mathbf{r}, [\hat{\rho}]) = \log[\hat{\rho}(\mathbf{r}) v(\mathbf{r}, [\hat{\rho}])]$ is a nonequilibrium chemical potential, and $\boldsymbol{\Lambda}$ is a centered Gaussian white noise of unit variance and delta correlated in space. The derivation of

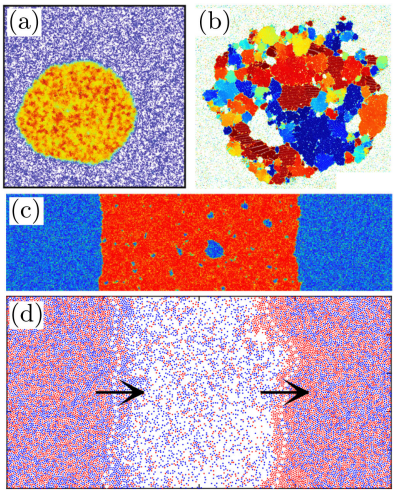

FIG. 22. (a) MIPS in ABPs interacting via quorum sensing showing a liquid-gas phase separation. From Solon, Cates, and Tailleur, 2015. (b) MIPS in ABPs interacting via a stiff repulsion showing a mosaic of hexatic domains and gas inclusions in the dense phase. The color and brightness indicate the direction of the hexatic order. From Caporusso *et al.*, 2020. (c) MIPS in ABPs interacting via harmonic repulsion showing a distribution of gas bubbles in the dense phase. The midregion (warmer colors) has a higher density. From Shi *et al.*, 2020. (d) MIPS in a mixture of ABPs and passive Brownian particles showing propagating interfaces in the direction indicated by the black arrows. From Wysocki, Winkler, and Gompper, 2016.

Eq. (A1) relies on a diffusive approximation of the microscopic run-and-tumble dynamics (Tailleur and Cates, 2008; Cates and Tailleur, 2013; Solon, Cates, and Tailleur, 2015) and on stochastic calculus (Dean, 1996; Solon, Cates, and Tailleur, 2015).

In a system with a homogeneous density ρ_0, the chemical potential can be written as $\mathfrak{u} = \log[\rho_0 v(\mathbf{r}, [\rho_0])] \equiv f'(\rho_0)$, where $f(\rho_0)$ is a Landau-like free energy density. For all density values such that $f''(\rho_0) < 0$, a homogeneous system is linearly unstable and separates into liquid and gas phases. This instability defines a spinodal region. To predict the coexisting "binodal" densities and the phase diagram of the system, one needs to consider inhomogeneous density profiles. The mapping onto an equilibrium theory then breaks down because $\mathfrak{u}$ generally cannot be written as the functional derivative of a free energy $\mathcal{F}[\rho]$. To leading order in a gradient expansion, however, a predictive theory can be formulated to determine the phase diagram (Solon *et al.*, 2018a, 2018b).

Active particles interacting via pairwise forces (PFAPs) provide another system for which an explicit coarse graining of the microscopic dynamics is possible. In the presence of repulsive interactions, it has led to a predictive theory for MIPS. This case is significantly more involved than QSAPs, but a series of articles have led to an understanding of the spinodal instability, first, and more recently to the prediction of the binodals (Fily and Marchetti, 2012; Redner, Hagan, and Baskaran, 2013; Stenhammar *et al.*, 2014; Solon, Stenhammar *et al.*, 2015; Takatori and Brady, 2015; Solon *et al.*, 2018a, 2018b; Speck, 2021).

An alternative route to account for MIPS is to follow phenomenological approaches and construct a hydrodynamic description for a fluctuating coarse-grained density field ρ that includes all terms allowed by symmetry (Wittkowski *et al.*, 2014). At the fourth order in a gradient expansion, one obtains active model B+ dynamics (Tjhung, Nardini, and Cates, 2018),

$$\partial_t \rho = -\boldsymbol{\nabla} \cdot [\mathbf{J} + \sqrt{2DM}\boldsymbol{\Lambda}], \tag{A3}$$

$$\mathbf{J}/M = -\boldsymbol{\nabla}\left[\frac{\delta \mathcal{F}}{\delta \rho} + \lambda |\boldsymbol{\nabla}\rho|^2\right] + \zeta(\boldsymbol{\nabla}^2\rho)\boldsymbol{\nabla}\rho, \tag{A4}$$

where $\mathcal{F} = \int d^d\mathbf{r}[f(\rho) + \kappa|\boldsymbol{\nabla}\rho|^2]$ and $f(\rho)$ again plays the role of a Landau free energy density. All coefficients D, M, κ, λ, and ζ depend in principle on ρ. The λ and ζ terms both break time-reversal symmetry (Nardini *et al.*, 2017; Tjhung, Nardini, and Cates, 2018), and the dynamics in Eqs. (A3) and (A4) cannot be derived from a free energy as in regular model B. Active model B+ is thus a generalization of Eq. (A1), which accounts for MIPS in a broader set of systems. Using the methods developed by Solon *et al.* (2018a, 2018b), it is again possible to predict the coexisting densities of a fully phase-separated system. An interesting difference from equilibrium physics is that the interfacial terms contribute to the results (Wittkowski *et al.*, 2014).

2. Beyond the simple MIPS scenario

Equations (A3) and (A4) predict a richer physics than the previously discussed simple MIPS scenario: for large values of $|\zeta|$, one observes a reversed Ostwald ripening whereby small droplets grow at the expense of larger ones (Tjhung, Nardini, and Cates, 2018). In the phase coexistence regime, this leads to a dense phase that contains droplets of the dilute phase evolving with complex dynamics. This is reminiscent of what has been observed in simulations of PFAPs, where the droplet sizes are found to be algebraically distributed, leading to the critical dense phase (Caporusso *et al.*, 2020; Shi *et al.*, 2020) shown in Fig. 22(c).

Besides the nature of the phase-separated state, the critical properties of MIPS have also attracted attention. Conflicting results have been reported regarding the critical point (Speck, 2022a). It has been measured and argued to have exponents in either the Ising universality class (Partridge and Lee, 2019; Maggi *et al.*, 2021, 2022) or another one (Caballero, Nardini, and Cates, 2018; Siebert *et al.*, 2018), and the effect, or absence thereof, of bubbles on the critical point remains unclear (Caballero, Nardini, and Cates, 2018).

The previously described microscopic systems display interesting properties beyond those captured solely by the dynamics of their density field, and thus fall outside the scope of this Colloquium. For instance, the dense phases observed in $d = 2$ simulations of PFAPs have revealed a rich structure: they are found either in a disordered liquid form (Fily and Marchetti, 2012) for soft repulsive potentials or as a mosaic of hexatic domains with different orientations for stiffer ones; see Redner, Hagan, and Baskaran (2013) and Digregorio *et al.* (2018) and Fig. 22(b). Furthermore, the hexatic phase observed in the passive limit of this system survives the addition of activity (Digregorio *et al.*, 2018) and has recently attracted substantial attention (Digregorio *et al.*, 2019). At high density, active systems exhibit a glassy dynamics that has been observed experimentally (Angelini *et al.*, 2011; Garcia *et al.*, 2015; Klongvessa *et al.*, 2019) and numerically (Levis and Berthier, 2015; Berthier, Flenner, and Szamel, 2017; Berthier, Flenner, and Szamel, 2019; Klongvessa *et al.*, 2019).

Finally, rich physical phenomena occur in mixtures of scalar active systems. For example, mixtures of active and passive particles interacting via pairwise repulsion can demix (Weber, Weber, and Frey, 2016; Ilker and Joanny, 2020) or jointly undergo MIPS (Stenhammar *et al.*, 2015), while mixed species of QSAPs can either segregate or colocalize (Curatolo *et al.*, 2020). Out of equilibrium, one would generically expect the interactions between two species to be nonreciprocal. Even for PFAPs, which obey Newton's third law of action and reaction microscopically, the large-scale description of a mixture of active and passive particles features nonreciprocal couplings (Wittkowski, Stenhammar, and Cates, 2017). When strong enough, the nonreciprocity gives rise to propagating patterns, as shown using a phenomenological theory (Saha, Agudo-Canalejo, and Golestanian, 2020; You, Baskaran, and Marchetti, 2020) and observed in mixtures of active and passive ABPs (Wysocki, Winkler, and Gompper, 2016) [see Fig. 22(d)], as well as for mixtures of QSAPs (Dinelli *et al.*, 2022).

REFERENCES

Adachi, K., and K. Kawaguchi, 2020, "Universality of active and passive phase separation in a lattice model," arXiv:2012.02517.

Agranov, T., S. Ro, Y. Kafri, and V. Lecomte, 2021, "Exact fluctuating hydrodynamics of active lattice gases—Typical fluctuations," J. Stat. Mech. 083208.

Aharony, A., Y. Imry, and S. Ma, 1976, "Lowering of Dimensionality in Phase Transitions with Random Fields," Phys. Rev. Lett. **37**, 1364–1367.

Ai, B., and J. Wu, 2014, "Transport of active ellipsoidal particles in ratchet potentials," J. Chem. Phys. **140**, 094103.

Aizenman, M., and J. Wehr, 1989, "Rounding of First-Order Phase Transitions in Systems with Quenched Disorder," Phys. Rev. Lett. **62**, 2503–2506.

Anderson, C. J., G. Briand, O. Dauchot, and A. Fernández-Nieves, 2022, "Polymer-chain configurations in active and passive baths," Phys. Rev. E **106**, 064606.

Angelani, L., A. Costanzo, and R. Di Leonardo, 2011, "Active ratchets," Europhys. Lett. **96**, 68002.

Angelani, L., and R. Di Leonardo, 2010, "Geometrically biased random walks in bacteria-driven micro-shuttles," New J. Phys. **12**, 113017.

Angelani, L., R. Di Leonardo, and G. Ruocco, 2009, "Self-Starting Micromotors in a Bacterial Bath," Phys. Rev. Lett. **102**, 048104.

Angelini, T. E., E. Hannezo, X. Trepat, M. Marquez, J. J. Fredberg, and D. A. Weitz, 2011, "Glass-like dynamics of collective cell migration," Proc. Natl. Acad. Sci. U.S.A. **108**, 4714–4719.

Ao, P., 2004, "Potential in stochastic differential equations: Novel construction," J. Phys. A **37**, L25–L30.

Arnoulx de Pirey, T., and F. van Wijland, 2023, "A run-and-tumble particle around a spherical obstacle: Steady-state distribution far-from-equilibrium," arXiv:2303.00331.

Baek, Y., A. P. Solon, X. Xu, N. Nikola, and Y. Kafri, 2018, "Generic Long-Range Interactions between Passive Bodies in an Active Fluid," Phys. Rev. Lett. **120**, 058002.

Basu, U., S. N. Majumdar, A. Rosso, S. Sabhapandit, and G. Schehr, 2020, "Exact stationary state of a run-and-tumble particle with three internal states in a harmonic trap," J. Phys. A **53**, 09LT01.

Bäuerle, T., A. Fischer, T. Speck, and C. Bechinger, 2018, "Self-organization of active particles by quorum sensing rules," Nat. Commun. **9**, 3232.

Bechinger, C., R. Di Leonardo, H. Löwen, C. Reichhardt, G. Volpe, and G. Volpe, 2016, "Active particles in complex and crowded environments," Rev. Mod. Phys. **88**, 045006.

Belanger, D. P., A. R. King, V. Jaccarino, and J. L. Cardy, 1983, "Random-field critical behavior of a $d = 3$ Ising system," Phys. Rev. B **28**, 2522–2526.

Ben Dor, Y., Y. Kafri, M. Kardar, and J. Tailleur, 2022, "Passive objects in confined active fluids: A localization transition," Phys. Rev. E **106**, 044604.

Ben Dor, Y., S. Ro, Y. Kafri, M. Kardar, and J. Tailleur, 2022, "Disordered boundaries destroy bulk phase separation in scalar active matter," Phys. Rev. E **105**, 044603.

Ben Dor, Y., E. Woillez, Y. Kafri, M. Kardar, and A. P. Solon, 2019, "Ramifications of disorder on active particles in one dimension," Phys. Rev. E **100**, 052610.

Benvegnen, B., O. Granek, S. Ro, R. Yaacoby, H. Chaté, Y. Kafri, D. Mukamel, A. Solon, and J. Tailleur, 2023, "Metastability of discrete-symmetry flocks," arXiv:2306.01156.

Ben Zion, M. Y., J. Fersula, N. Bredeche, and O. Dauchot, 2023, "Morphological computation and decentralized learning in a swarm of sterically interacting robots," Sci. Rob. **8**, eabo6140.

Berg, H. C., 2004, *E. coli in Motion* (Springer, New York).

Berthier, L., E. Flenner, and G. Szamel, 2017, "How active forces influence nonequilibrium glass transitions," New J. Phys. **19**, 125006.

Berthier, L., E. Flenner, and G. Szamel, 2019, "Glassy dynamics in dense systems of active particles," J. Chem. Phys. **150**, 200901.

Bettolo Marconi Marini, U., C. Maggi, and S. Melchionna, 2016, "Pressure and surface tension of an active simple liquid: A comparison between kinetic, mechanical and free-energy based approaches," Soft Matter **12**, 5727–5738.

Bhattacharjee, T., and S. S. Datta, 2019, "Bacterial hopping and trapping in porous media," Nat. Commun. **10**, 2075.

Bialké, J., J. T. Siebert, H. Löwen, and T. Speck, 2015, "Negative Interfacial Tension in Phase-Separated Active Brownian Particles," Phys. Rev. Lett. **115**, 098301.

Bouchaud, J. P., A. Comtet, A. Georges, and P. Le Doussal, 1990, "Classical diffusion of a particle in a one-dimensional random force field," Ann. Phys. (N.Y.) **201**, 285–341.

Brenner, M. P., L. S. Levitov, and E. O. Budrene, 1998, "Physical mechanisms for chemotactic pattern formation by bacteria," Biophys. J. **74**, 1677–1693.

Bricard, A., J. Caussin, N. Desreumaux, O. Dauchot, and D. Bartolo, 2013, "Emergence of macroscopic directed motion in populations of motile colloids," Nature (London) **503**, 95–98.

Bricmont, J., and A. Kupiainen, 1987, "Lower Critical Dimension for the Random-Field Ising Model," Phys. Rev. Lett. **59**, 1829–1832.

Burkholder, E. W., and J. F. Brady, 2017, "Tracer diffusion in active suspensions," Phys. Rev. E **95**, 052605.

Burkholder, E. W., and J. F. Brady, 2019, "Fluctuation-dissipation in active matter," J. Chem. Phys. **150**, 184901.

Buttinoni, I., J. Bialké, F. Kümmel, H. Löwen, C. Bechinger, and T. Speck, 2013, "Dynamical Clustering and Phase Separation in Suspensions of Self-Propelled Colloidal Particles," Phys. Rev. Lett. **110**, 238301.

Caballero, F., C. Nardini, and M. E. Cates, 2018, "From bulk to microphase separation in scalar active matter: A perturbative renormalization group analysis," J. Stat. Mech. 123208.

Caporusso, C. B., P. Digregorio, D. Levis, L. F. Cugliandolo, and G. Gonnella, 2020, "Motility-Induced Microphase and Macrophase Separation in a Two-Dimensional Active Brownian Particle System," Phys. Rev. Lett. **125**, 178004.

Cates, M. E., and J. Tailleur, 2013, "When are active Brownian particles and run-and-tumble particles equivalent? Consequences for motility-induced phase separation," Europhys. Lett. **101**, 20010.

Cates, M. E., and J. Tailleur, 2015, "Motility-induced phase separation," Annu. Rev. Condens. Matter Phys. **6**, 219–244.

Chardac, A., S. Shankar, M. C. Marchetti, and D. Bartolo, 2021, "Emergence of dynamic vortex glasses in disordered polar active fluids," Proc. Natl. Acad. Sci. U.S.A. **118**, e2018218118.

Chaté, H., 2020, "Dry aligning dilute active matter," Annu. Rev. Condens. Matter Phys. **11**, 189–212.

Chen, D. T. N., A. W. C. Lau, L. A. Hough, M. F. Islam, M. Goulian, T. C. Lubensky, and A. G. Yodh, 2007, "Fluctuations and Rheology in Active Bacterial Suspensions," Phys. Rev. Lett. **99**, 148302.

Chun, H., Q. Gao, and J. M. Horowitz, 2021, "Nonequilibrium Green-Kubo relations for hydrodynamic transport from an equilibrium-like fluctuation-response equality," Phys. Rev. Res. **3**, 043172.

Codina, J., B. Mahault, H. Chaté, J. Dobnikar, I. Pagonabarraga, and X. Shi, 2022, "Small Obstacle in a Large Polar Flock," Phys. Rev. Lett. **128**, 218001.

Creppy, A., E. Clément, C. Douarche, M. V. D'Angelo, and H. Auradou, 2019, "Effect of motility on the transport of bacteria

populations through a porous medium," Phys. Rev. Fluids **4**, 013102.
Curatolo, A. I., N. Zhou, Y. Zhao, C. Liu, A. Daerr, J. Tailleur, and J. Huang, 2020, "Cooperative pattern formation in multi-component bacterial systems through reciprocal motility regulation," Nat. Phys. **16**, 1152–1157.
D'Alessandro, J., A. P. Solon, Y. Hayakawa, C. Anjard, F. Detcheverry, J. Rieu, and C. Rivière, 2017, "Contact enhancement of locomotion in spreading cell colonies," Nat. Phys. **13**, 999–1005.
D'Alessio, L., Y. Kafri, and A. Polkovnikov, 2016, "Negative mass corrections in a dissipative stochastic environment," J. Stat. Mech. 023105.
Daniels, R., J. Vanderleyden, and J. Michiels, 2004, "Quorum sensing and swarming migration in bacteria," FEMS Microbiol. Rev. **28**, 261–289.
Datta, A., P. Pietzonka, and A. C. Barato, 2022, "Second Law for Active Heat Engines," Phys. Rev. X **12**, 031034.
Dean, D. S., 1996, "Langevin equation for the density of a system of interacting Langevin processes," J. Phys. A **29**, L613–L617.
de Pirey, T. A., Y. Kafri, and S. Ramaswamy, 2024, "The anomalous long-ranged influence of an inclusion in momentum-conserving active fluids," arXiv:2402.12996.
Derrida, B., 1983, "Velocity and diffusion constant of a periodic one-dimensional hopping model," J. Stat. Phys. **31**, 433–450.
Derrida, B., and Y. Pomeau, 1982, "Classical Diffusion on a Random Chain," Phys. Rev. Lett. **48**, 627–630.
Deseigne, J., O. Dauchot, and H. Chaté, 2010, "Collective Motion of Vibrated Polar Disks," Phys. Rev. Lett. **105**, 098001.
Digregorio, P., D. Levis, A. Suma, L. F. Cugliandolo, G. Gonnella, and I. Pagonabarraga, 2018, "Full Phase Diagram of Active Brownian Disks: From Melting to Motility-Induced Phase Separation," Phys. Rev. Lett. **121**, 098003.
Digregorio, P., D. Levis, A. Suma, L. F. Cugliandolo, G. Gonnella, and I. Pagonabarraga, 2019, "2D melting and motility induced phase separation in active Brownian hard disks and dumbbells," J. Phys. Conf. Ser. **1163**, 012073.
Di Leonardo, R., L. Angelani, D. Dell'Arciprete, G. Ruocco, V. Iebba, S. Schippa, M. P. Conte, F. Mecarini, F. De Angelis, and E. Di Fabrizio, 2010, "Bacterial ratchet motors," Proc. Natl. Acad. Sci. U.S.A. **107**, 9541–9545.
Dinelli, A., J. O'Byrne, A. Curatolo, Y. Zhao, P. Sollich, and J. Tailleur, 2022, "Non-reciprocity across scales in active mixtures," arXiv:2203.07757.
Dittrich, F., T. Speck, and P. Virnau, 2021, "Critical behavior in active lattice models of motility-induced phase separation," Eur. Phys. J. E **44**, 53.
Dolai, P., S. Krekels, and C. Maes, 2022, "Inducing a bound state between active particles," Phys. Rev. E **105**, 044605.
Duan, Y., B. Mahault, Y. Ma, X. Shi, and H. Chaté, 2021, "Breakdown of Ergodicity and Self-Averaging in Polar Flocks with Quenched Disorder," Phys. Rev. Lett. **126**, 178001.
Ekeh, T., M. E. Cates, and É. Fodor, 2020, "Thermodynamic cycles with active matter," Phys. Rev. E **102**, 010101.
Elgeti, J., and G. Gompper, 2016, "Microswimmers near surfaces," Eur. Phys. J. Special Topics **225**, 2333–2352.
Engebrecht, J., and M. Silverman, 1984, "Identification of genes and gene products necessary for bacterial bioluminescence," Proc. Natl. Acad. Sci. U.S.A. **81**, 4154–4158.
Falasco, G., F. Baldovin, K. Kroy, and M. Baiesi, 2016, "Mesoscopic virial equation for nonequilibrium statistical mechanics," New J. Phys. **18**, 093043.
Fausti, G., E. Tjhung, M. Cates, and C. Nardini, 2021, "Capillary Interfacial Tension in Active Phase Separation," Phys. Rev. Lett. **127**, 068001.
Feng, M., and Z. Hou, 2023, "Unraveling on kinesin acceleration in intracellular environments: A theory for active bath," Phys. Rev. Res. **5**, 013206.
Fily, Y., A. Baskaran, and M. F. Hagan, 2014, "Dynamics of self-propelled particles under strong confinement," Soft Matter **10**, 5609–5617.
Fily, Y., A. Baskaran, and M. F. Hagan, 2015, "Dynamics and density distribution of strongly confined noninteracting nonaligning self-propelled particles in a nonconvex boundary," Phys. Rev. E **91**, 012125.
Fily, Y., and M. C. Marchetti, 2012, "Athermal Phase Separation of Self-Propelled Particles with No Alignment," Phys. Rev. Lett. **108**, 235702.
Fisher, D. S., 1984, "Random walks in random environments," Phys. Rev. A **30**, 960–964.
Fisher, D. S., J. Fröhlich, and T. Spencer, 1984, "The Ising model in a random magnetic field," J. Stat. Phys. **34**, 863–870.
Fodor, É., and M. E. Cates, 2021, "Active engines: Thermodynamics moves forward," Europhys. Lett. **134**, 10003.
Fodor, É., and C. Marchetti, 2018, "The statistical physics of active matter: From self-catalytic colloids to living cells," Physica (Amsterdam) **504A**, 106–120.
Fodor, É., C. Nardini, M. E. Cates, J. Tailleur, P. Visco, and F. van Wijland, 2016, "How Far from Equilibrium Is Active Matter?," Phys. Rev. Lett. **117**, 038103.
Frangipane, G., D. Dell'Arciprete, S. Petracchini, C. Maggi, F. Saglimbeni, S. Bianchi, G. Vizsnyiczai, M. L. Bernardini, and R. Di Leonardo, 2018, "Dynamic density shaping of photokinetic *E. coli*," eLife **7**, e36608.
Fruchart, M., R. Hanai, P. B. Littlewood, and V. Vitelli, 2021, "Non-reciprocal phase transitions," Nature (London) **592**, 363–369.
Fuqua, W. C., S. C. Winans, and E. P. Greenberg, 1994, "Quorum sensing in bacteria: The LuxR-LuxI family of cell density-responsive transcriptional regulators," J. Bacteriol. **176**, 269–275.
Galajda, P., J. Keymer, P. Chaikin, and R. Austin, 2007, "A wall of funnels concentrates swimming bacteria," J. Bacteriol. **189**, 8704–8707.
Garcia, S., E. Hannezo, J. Elgeti, J. Joanny, P. Silberzan, and N. S. Gov, 2015, "Physics of active jamming during collective cellular motion in a monolayer," Proc. Natl. Acad. Sci. U.S.A. **112**, 15314–15319.
Ginot, F., A. Solon, Y. Kafri, C. Ybert, J. Tailleur, and C. Cottin-Bizonne, 2018, "Sedimentation of self-propelled Janus colloids: Polarization and pressure," New J. Phys. **20**, 115001.
Glaus, U., 1986, "Correlations in the two-dimensional random-field Ising model," Phys. Rev. B **34**, 3203–3211.
Granek, O., 2023, "Universal fluctuations of local measurement in low-dimensional systems," arXiv:2308.08595.
Granek, O., Y. Baek, Y. Kafri, and A. P. Solon, 2020, "Bodies in an interacting active fluid: Far-field influence of a single body and interaction between two bodies," J. Stat. Mech. 063211.
Granek, O., Y. Kafri, and J. Tailleur, 2022, "Anomalous Transport of Tracers in Active Baths," Phys. Rev. Lett. **129**, 038001.
Hammer, B. K., and B. L. Bassler, 2003, "Quorum sensing controls biofilm formation in *Vibrio cholerae*," Mol. Microbiol. **50**, 101–104.
Han, M., M. Fruchart, C. Scheibner, S. Vaikuntanathan, J. J. De Pablo, and V. Vitelli, 2021, "Fluctuating hydrodynamics of chiral active fluids," Nat. Phys. **17**, 1260–1269.

Hänggi, P, and P. Jung, 1994, "Colored noise in dynamical systems," Adv. Chem. Phys. **89**, 239–326.
Hanna, S., W. Hess, and R. Klein, 1981, "The velocity autocorrelation function of an overdamped Brownian system with hard-core intraction," J. Phys. A **14**, L493–L498.
Harder, J., C. Valeriani, and A. Cacciuto, 2014, "Activity-induced collapse and reexpansion of rigid polymers," Phys. Rev. E **90**, 062312.
Hennes, M., K. Wolff, and H. Stark, 2014, "Self-Induced Polar Order of Active Brownian Particles in a Harmonic Trap," Phys. Rev. Lett. **112**, 238104.
Hermann, S., D. de las Heras, and M. Schmidt, 2019, "Non-negative Interfacial Tension in Phase-Separated Active Brownian Particles," Phys. Rev. Lett. **123**, 268002.
Herminghaus, S., C. C. Maass, C. Krüger, S. Thutupalli, L. Goehring, and C. Bahr, 2014, "Interfacial mechanisms in active emulsions," Soft Matter **10**, 7008–7022.
Holubec, V., and R. Marathe, 2020, "Underdamped active Brownian heat engine," Phys. Rev. E **102**, 060101(R).
Howse, J. R., R. A. L. Jones, A. J. Ryan, T. Gough, R. Vafabakhsh, and R. Golestanian, 2007, "Self-Motile Colloidal Particles: From Directed Propulsion to Random Walk," Phys. Rev. Lett. **99**, 048102.
Ilker, E., and J. Joanny, 2020, "Phase separation and nucleation in mixtures of particles with different temperatures," Phys. Rev. Res. **2**, 023200.
Imbrie, J. Z., 1984, "Lower Critical Dimension of the Random-Field Ising Model," Phys. Rev. Lett. **53**, 1747–1750.
Imbrie, J. Z., 1985, "The ground state of the three-dimensional random-field Ising model," Commun. Math. Phys. **98**, 145–176.
Imry, Y., and S. Ma, 1975, "Random-Field Instability of the Ordered State of Continuous Symmetry," Phys. Rev. Lett. **35**, 1399–1401.
Izzet, A., P. G. Moerman, P. Gross, J. Groenewold, A. D. Hollingsworth, J. Bibette, and J. Brujic, 2020, "Tunable Persistent Random Walk in Swimming Droplets," Phys. Rev. X **10**, 021035.
Jayaram, A., and T. Speck, 2023, "Effective dynamics and fluctuations of a trapped probe moving in a fluid of active hard discs," Europhys. Lett. **143**, 17005.
Junot, G., G. Briand, R. Ledesma-Alonso, and O. Dauchot, 2017, "Active versus Passive Hard Disks against a Membrane: Mechanical Pressure and Instability," Phys. Rev. Lett. **119**, 028002.
Kaiser, A., A. Peshkov, A. Sokolov, B. ten Hagen, H. Löwen, and I. S. Aranson, 2014, "Transport Powered by Bacterial Turbulence," Phys. Rev. Lett. **112**, 158101.
Kaiser, A., H. H. Wensink, and H. Löwen, 2012, "How to Capture Active Particles," Phys. Rev. Lett. **108**, 268307.
Kanazawa, K., T. G. Sano, A. Cairoli, and A. Baule, 2020, "Loopy Lévy flights enhance tracer diffusion in active suspensions," Nature (London) **579**, 364–367.
Kardar, M., 2007, *Statistical Physics of Fields* (Cambridge University Press, Cambridge, England).
Kim, K., Y. Choe, and Y. Baek, 2023, "Generic symmetry-breaking motility in active fluids," arXiv:2304.01645.
Klongvessa, N., F. Ginot, C. Ybert, C. Cottin-Bizonne, and M. Leocmach, 2019, "Active Glass: Ergodicity Breaking Dramatically Affects Response to Self-Propulsion," Phys. Rev. Lett. **123**, 248004.
Knežević, M, and H. Stark, 2020, "Effective Langevin equations for a polar tracer in an active bath," New J. Phys. **22**, 113025.
Knežević, M,, L. E. Avilés Podgurski, and H. Stark, 2021, "Oscillatory active microrheology of active suspensions," Sci. Rep. **11**, 22706.
Koumakis, N., A. Lepore, C. Maggi, and R. Di Leonardo, 2013, "Targeted delivery of colloids by swimming bacteria," Nat. Commun. **4**, 2588.
Kourbane-Houssene, M., C. Erignoux, T. Bodineau, and J. Tailleur, 2018, "Exact Hydrodynamic Description of Active Lattice Gases," Phys. Rev. Lett. **120**, 268003.
Kurihara, T., M. Aridome, H. Ayade, I. Zaid, and D. Mizuno, 2017, "Non-Gaussian limit fluctuations in active swimmer suspensions," Phys. Rev. E **95**, 030601.
Kurtuldu, H., J. S. Guasto, K. A. Johnson, and J. P. Gollub, 2011, "Enhancement of biomixing by swimming algal cells in two-dimensional films," Proc. Natl. Acad. Sci. U.S.A. **108**, 10391–10395.
Kwon, C., P. Ao, and D. J. Thouless, 2005, "Structure of stochastic dynamics near fixed points," Proc. Natl. Acad. Sci. U.S.A. **102**, 13029–13033.
Lauersdorf, N., T. Kolb, M. Moradi, E. Nazockdast, and D. Klotsa, 2021, "Phase behavior and surface tension of soft active Brownian particles," Soft Matter **17**, 6337–6351.
Lauga, E., and T. R. Powers, 2009, "The hydrodynamics of swimming microorganisms," Rep. Prog. Phys. **72**, 096601.
Leptos, K. C., J. S. Guasto, J. P. Gollub, A. I. Pesci, and R. E. Goldstein, 2009, "Dynamics of Enhanced Tracer Diffusion in Suspensions of Swimming Eukaryotic Microorganisms," Phys. Rev. Lett. **103**, 198103.
Levis, D., and L. Berthier, 2015, "From single-particle to collective effective temperatures in an active fluid of self-propelled particles," Europhys. Lett. **111**, 60006.
Li, H., and H. P. Zhang, 2013, "Asymmetric gear rectifies random robot motion," Europhys. Lett. **102**, 50007.
Liu, C., *et al.*, 2011, "Sequential establishment of stripe patterns in an expanding cell population," Science **334**, 238–241.
Liu, G., A. Patch, F. Bahar, D. Yllanes, R. D. Welch, M. C. Marchetti, S. Thutupalli, and J. W. Shaevitz, 2019, "Self-Driven Phase Transitions Drive *Myxococcus xanthus* Fruiting Body Formation," Phys. Rev. Lett. **122**, 248102.
Liu, Z. T., Y. Shi, Y. Zhao, H. Chaté, X. Shi, and T. H. Zhang, 2021, "Activity waves and freestanding vortices in populations of subcritical Quincke rollers," Proc. Natl. Acad. Sci. U.S.A. **118**, e2104724118.
Maes, C., 2020, "Fluctuating Motion in an Active Environment," Phys. Rev. Lett. **125**, 208001.
Maggi, C., L. Angelani, G. Frangipane, and R. Di Leonardo, 2018, "Currents and flux-inversion in photokinetic active particles," Soft Matter **14**, 4958–4962.
Maggi, C., N. Gnan, M. Paoluzzi, E. Zaccarelli, and A. Crisanti, 2022, "Critical active dynamics is captured by a colored-noise driven field theory," Commun. Phys. **5**, 55.
Maggi, C., U. M. B. Marconi, N. Gnan, and R. Di Leonardo, 2015, "Multidimensional stationary probability distribution for interacting active particles," Sci. Rep. **5**, 10742.
Maggi, C., M. Paoluzzi, L. Angelani, and R. Di Leonardo, 2017, "Memory-less response and violation of the fluctuation-dissipation theorem in colloids suspended in an active bath," Sci. Rep. **7**, 17588.
Maggi, C., M. Paoluzzi, A. Crisanti, E. Zaccarelli, and N. Gnan, 2021, "Universality class of the motility-induced critical point in large scale off-lattice simulations of active particles," Soft Matter **17**, 3807–3812.
Maggi, C., F. Saglimbeni, M. Dipalo, F. De Angelis, and R. Di Leonardo, 2015, "Micromotors with asymmetric shape that efficiently convert light into work by thermocapillary effects," Nat. Commun. **6**, 7855.

Maitra, A., 2023, "Two-dimensional long-range uniaxial order in three-dimensional active fluids," Nat. Phys. **19**, 733–740.
Malakar, K., A. Das, A. Kundu, K. V. Kumar, and A. Dhar, 2020, "Steady state of an active Brownian particle in a two-dimensional harmonic trap," Phys. Rev. E **101**, 022610.
Mallory, S. A., A. Šarić, C. Valeriani, and A. Cacciuto, 2014, "Anomalous thermomechanical properties of a self-propelled colloidal fluid," Phys. Rev. E **89**, 052303.
Mallory, S. A., C. Valeriani, and A. Cacciuto, 2014, "Curvature-induced activation of a passive tracer in an active bath," Phys. Rev. E **90**, 032309.
Marchetti, M. C., J. F. Joanny, S. Ramaswamy, T. B. Liverpool, J. Prost, M. Rao, and R. A. Simha, 2013, "Hydrodynamics of soft active matter," Rev. Mod. Phys. **85**, 1143–1189.
Martin, D., J. O'Byrne, M. E. Cates, É. Fodor, C. Nardini, J. Tailleur, and F. van Wijland, 2021, "Statistical mechanics of active Ornstein-Uhlenbeck particles," Phys. Rev. E **103**, 032607.
Martin, D., D. Seara, Y. Avni, M. Fruchart, and V. Vitelli, 2023, "An exact model for the transition to collective motion in nonreciprocal active matter," arXiv:2307.08251.
Massana-Cid, H., C. Maggi, G. Frangipane, and R. Di Leonardo, 2022, "Rectification and confinement of photokinetic bacteria in an optical feedback loop," Nat. Commun. **13**, 2740.
Miller, M. B., and B. L. Bassler, 2001, "Quorum sensing in bacteria," Annu. Rev. Microbiol. **55**, 165–199.
Mognetti, B. M., A. Šarić, S. Angioletti-Uberti, A. Cacciuto, C. Valeriani, and D. Frenkel, 2013, "Living Clusters and Crystals from Low-Density Suspensions of Active Colloids," Phys. Rev. Lett. **111**, 245702.
Morin, A., N. Desreumaux, J. Caussin, and D. Bartolo, 2017, "Distortion and destruction of colloidal flocks in disordered environments," Nat. Phys. **13**, 63–67.
Narayan, V., S. Ramaswamy, and N. Menon, 2007, "Long-lived giant number fluctuations in a swarming granular nematic," Science **317**, 105–108.
Nardini, C., É. Fodor, E. Tjhung, F. van Wijland, J. Tailleur, and M. E. Cates, 2017, "Entropy Production in Field Theories without Time-Reversal Symmetry: Quantifying the Non-Equilibrium Character of Active Matter," Phys. Rev. X **7**, 021007.
Nealson, K. H., T. Platt, and J. W. Hastings, 1970, "Cellular control of the synthesis and activity of the bacterial luminescent system," J. Bacteriol. **104**, 313–322.
Ni, R., M. A. Cohen Stuart, and P. G. Bolhuis, 2015, "Tunable Long Range Forces Mediated by Self-Propelled Colloidal Hard Spheres," Phys. Rev. Lett. **114**, 018302.
Nikola, N., A. P. Solon, Y. Kafri, M. Kardar, J. Tailleur, and R. Voituriez, 2016, "Active Particles with Soft and Curved Walls: Equation of State, Ratchets, and Instabilities," Phys. Rev. Lett. **117**, 098001.
Nishiguchi, D., and M. Sano, 2015, "Mesoscopic turbulence and local order in Janus particles self-propelling under an ac electric field," Phys. Rev. E **92**, 052309.
O'Byrne, J., A. Solon, J. Tailleur, and Y. Zhao, 2023, "An introduction to motility-induced phase separation," in *Out-of-Equilibrium Soft Matter: Active Fluids*, Soft Matter Series, edited by Christina Kurzthaler, Luigi Gentile, and Howard A. Stone (Royal Society of Chemistry, London), Chap. 4.
O'Byrne, J., and J. Tailleur, 2020, "Lamellar to Micellar Phases and Beyond: When Tactic Active Systems Admit Free Energy Functionals," Phys. Rev. Lett. **125**, 208003.
Omar, A. K., H. Row, S. A. Mallory, and J. F. Brady, 2023, "Mechanical theory of nonequilibrium coexistence and motility-induced phase separation," *Proc. Natl. Acad. Sci. U.S.A.* 120, e2219900120.
Omar, A. K., Z. Wang, and J. F. Brady, 2020, "Microscopic origins of the swim pressure and the anomalous surface tension of active matter," Phys. Rev. E **101**, 012604.
Palacci, J., C. Cottin-Bizonne, C. Ybert, and L. Bocquet, 2010, "Sedimentation and Effective Temperature of Active Colloidal Suspensions," Phys. Rev. Lett. **105**, 088304.
Palacci, J., S. Sacanna, A. P. Steinberg, D. J. Pine, and P. M. Chaikin, 2013, "Living crystals of light-activated colloidal surfers," Science **339**, 936–940.
Paliwal, S., V. Prymidis, L. Filion, and M. Dijkstra, 2017, "Non-equilibrium surface tension of the vapour-liquid interface of active Lennard-Jones particles," J. Chem. Phys. **147**, 84902.
Paliwal, S., J. Rodenburg, R. van Roij, and M. Dijkstra, 2018, "Chemical potential in active systems: Predicting phase equilibrium from bulk equations of state?," New J. Phys. **20**, 015003.
Partridge, B., and C. F. Lee, 2019, "Critical Motility-Induced Phase Separation Belongs to the Ising Universality Class," Phys. Rev. Lett. **123**, 068002.
Paxton, W. F., K. C. Kistler, C. C. Olmeda, A. Sen, S. K. St. Angelo, Y. Cao, T. E. Mallouk, P. E. Lammert, and V. H. Crespi, 2004, "Catalytic nanomotors: autonomous movement of striped nanorods," J. Am. Chem. Soc. **126**, 13424–13431.
Peng, Z., and J. F. Brady, 2022, "Forced microrheology of active colloids," J. Rheol. **66**, 955–972.
Pérez-González, C., R. Alert, C. Blanch-Mercader, M. Gómez-González, T. Kolodziej, E. Bazellieres, J. Casademunt, and X. Trepat, 2019, "Active wetting of epithelial tissues," Nat. Phys. **15**, 79–88.
Peruani, F., and I. S. Aranson, 2018, "Cold Active Motion: How Time-Independent Disorder Affects the Motion of Self-Propelled Agents," Phys. Rev. Lett. **120**, 238101.
Pietzonka, P., É. Fodor, C. Lohrmann, M. E. Cates, and U. Seifert, 2019, "Autonomous Engines Driven by Active Matter: Energetics and Design Principles," Phys. Rev. X **9**, 041032.
Potiguar, F. Q., G. A. Farias, and W. P. Ferreira, 2014, "Self-propelled particle transport in regular arrays of rigid asymmetric obstacles," Phys. Rev. E **90**, 012307.
Ramaswamy, S., 2010, "The mechanics and statistics of active matter," Annu. Rev. Condens. Matter Phys. **1**, 323–345.
Redner, G. S., A. Baskaran, and M. F. Hagan, 2013, "Reentrant phase behavior in active colloids with attraction," Phys. Rev. E **88**, 012305.
Redner, G. S., M. F. Hagan, and A. Baskaran, 2013, "Structure and Dynamics of a Phase-Separating Active Colloidal Fluid," Phys. Rev. Lett. **110**, 055701.
Reichert, J., L. F. Granz, and T. Voigtmann, 2021, "Transport coefficients in dense active Brownian particle systems: Mode-coupling theory and simulation results," Eur. Phys. J. E **44**, 27.
Reichert, J., and T. Voigtmann, 2021, "Tracer dynamics in crowded active-particle suspensions," Soft Matter **17**, 10492–10504.
Reichhardt, C., and C. J. O. Reichhardt, 2013, "Active matter ratchets with an external drift," Phys. Rev. E **88**, 062310.
Reichhardt, C. J. O., and C. Reichhardt, 2017, "Ratchet effects in active matter systems," Annu. Rev. Condens. Matter Phys. **8**, 51–75.
Rizkallah, P., A. Sarracino, O. Bénichou, and P. Illien, 2023, "Absolute Negative Mobility of an Active Tracer in a Crowded Environment," Phys. Rev. Lett. **130**, 218201.
Ro, S., Y. Kafri, M. Kardar, and J. Tailleur, 2021, "Disorder-Induced Long-Ranged Correlations in Scalar Active Matter," Phys. Rev. Lett. **126**, 048003.

Rodenburg, J., S. Paliwal, M. de Jager, P. G. Bolhuis, M. Dijkstra, and R. van Roij, 2018, "Ratchet-induced variations in bulk states of an active ideal gas," J. Chem. Phys. **149**, 174910.

Rohwer, C. M., M. Kardar, and M. Krüger, 2020, "Activated diffusiophoresis," J. Chem. Phys. **152**, 084109.

Rohwer, C. M., A. Solon, M. Kardar, and M. Krüger, 2018, "Non-equilibrium forces following quenches in active and thermal matter," Phys. Rev. E **97**, 032125.

Romanczuk, P., M. Bär, W. Ebeling, B. Lindner, and L. Schimansky-Geier, 2012, "Active Brownian particles," Eur. Phys. J. Special Topics **202**, 1–162.

Saha, S., J. Agudo-Canalejo, and R. Golestanian, 2020, "Scalar Active Mixtures: The Nonreciprocal Cahn-Hilliard Model," Phys. Rev. X **10**, 041009.

Saha, S., R. Golestanian, and S. Ramaswamy, 2014, "Clusters, asters, and collective oscillations in chemotactic colloids," Phys. Rev. E **89**, 062316.

Sandford, C., A. Y. Grosberg, and J. Joanny, 2017, "Pressure and flow of exponentially self-correlated active particles," Phys. Rev. E **96**, 052605.

Sándor, C., A. Libál, C. Reichhardt, and C. O. Reichhardt, 2017, "Collective transport for active matter run-and-tumble disk systems on a traveling-wave substrate," Phys. Rev. E **95**, 012607.

Schmidt, F., H. Šípová-Jungová, M. Käll, A. Würger, and G. Volpe, 2021, "Non-equilibrium properties of an active nanoparticle in a harmonic potential," Nat. Commun. **12**, 1902.

Schnitzer, M. J., 1993, "Theory of continuum random walks and application to chemotaxis," Phys. Rev. E **48**, 2553–2568.

Sepúlveda, N., L. Petitjean, O. Cochet, E. Grasland-Mongrain, P. Silberzan, and V. Hakim, 2013, "Collective cell motion in an epithelial sheet can be quantitatively described by a stochastic interacting particle model," PLoS Comput. Biol. **9**, e1002944.

Sepúlveda, N., and R. Soto, 2018, "Universality of active wetting transitions," Phys. Rev. E **98**, 052141.

Sesé-Sansa, E., I. Pagonabarraga, and D. Levis, 2018, "Velocity alignment promotes motility-induced phase separation," Europhys. Lett. **124**, 30004.

Shea, J., G. Jung, and F. Schmid, 2022, "Passive probe particle in an active bath: Can we tell it is out of equilibrium?," Soft Matter **18**, 6965–6973.

Shi, X., G. Fausti, H. Chaté, C. Nardini, and A. Solon, 2020, "Self-Organized Critical Coexistence Phase in Repulsive Active Particles," Phys. Rev. Lett. **125**, 168001.

Shin, J., A. G. Cherstvy, W. K. Kim, and R. Metzler, 2015, "Facilitation of polymer looping and giant polymer diffusivity in crowded solutions of active particles," New J. Phys. **17**, 113008.

Siebert, J. T., F. Dittrich, F. Schmid, K. Binder, T. Speck, and P. Virnau, 2018, "Critical behavior of active Brownian particles," Phys. Rev. E **98**, 030601.

Sinai, Y. G., 1983, "The limiting behavior of a one-dimensional random walk in a random medium," Theory Probab. Appl. **27**, 256–268.

Sipos, O., K. Nagy, R. Di Leonardo, and P. Galajda, 2015, "Hydrodynamic Trapping of Swimming Bacteria by Convex Walls," Phys. Rev. Lett. **114**, 258104.

Smallenburg, F., and H. Löwen, 2015, "Swim pressure on walls with curves and corners," Phys. Rev. E **92**, 032304.

Smith, N. R., P. Le Doussal, S. N. Majumdar, and G. Schehr, 2022, "Exact position distribution of a harmonically confined run-and-tumble particle in two dimensions," Phys. Rev. E **106**, 054133.

Sokolov, A., M. M. Apodaca, B. A. Grzybowski, and I. S. Aranson, 2010, "Swimming bacteria power microscopic gears," Proc. Natl. Acad. Sci. U.S.A. **107**, 969–974.

Solon, A., and J. M. Horowitz, 2022, "On the Einstein relation between mobility and diffusion coefficient in an active bath," J. Phys. A **55**, 184002.

Solon, A. P., M. E. Cates, and J. Tailleur, 2015, "Active Brownian particles and run-and-tumble particles: A comparative study," Eur. Phys. J. Special Topics **224**, 1231–1262.

Solon, A. P., Y. Fily, A. Baskaran, M. E. Cates, Y. Kafri, M. Kardar, and J. Tailleur, 2015, "Pressure is not a state function for generic active fluids," Nat. Phys. **11**, 673–678.

Solon, A. P., J. Stenhammar, M. E. Cates, Y. Kafri, and J. Tailleur, 2018a, "Generalized thermodynamics of motility-induced phase separation: Phase equilibria, Laplace pressure, and change of ensembles," New J. Phys. **20**, 075001.

Solon, A. P., J. Stenhammar, M. E. Cates, Y. Kafri, and J. Tailleur, 2018b, "Generalized thermodynamics of phase equilibria in scalar active matter," Phys. Rev. E **97**, 020602.

Solon, A. P., J. Stenhammar, R. Wittkowski, M. Kardar, Y. Kafri, M. E. Cates, and J. Tailleur, 2015, "Pressure and Phase Equilibria in Interacting Active Brownian Spheres," Phys. Rev. Lett. **114**, 198301.

Spagnolie, S. E., G. R. Moreno-Flores, D. Bartolo, and E. Lauga, 2015, "Geometric capture and escape of a microswimmer colliding with an obstacle," Soft Matter **11**, 3396–3411.

Speck, T., 2021, "Coexistence of active Brownian disks: van der Waals theory and analytical results," Phys. Rev. E **103**, 012607.

Speck, T., 2022a, "Critical behavior of active Brownian particles: Connection to field theories," Phys. Rev. E **105**, 064601.

Speck, T., 2022b, "Efficiency of isothermal active matter engines: Strong driving beats weak driving," Phys. Rev. E **105**, L012601.

Speck, T., and A. Jayaram, 2021, "Vorticity Determines the Force on Bodies Immersed in Active Fluids," Phys. Rev. Lett. **126**, 138002.

Spera, G., C. Duclut, M. Durand, and J. Tailleur, 2023, "Nematic torques in scalar active matter: When fluctuations favor polar order and persistence," arXiv:2301.02568.

Spohn, H., 1980, "Kinetic equations from Hamiltonian dynamics: Markovian limits," Rev. Mod. Phys. **52**, 569–615.

Steffenoni, S., K. Kroy, and G. Falasco, 2016, "Interacting Brownian dynamics in a nonequilibrium particle bath," Phys. Rev. E **94**, 062139.

Stenhammar, J., 2021, "An introduction to motility-induced phase separation," arXiv:2112.05024.

Stenhammar, J., D. Marenduzzo, R. J. Allen, and M. E. Cates, 2014, "Phase behaviour of active Brownian particles: The role of dimensionality," Soft Matter **10**, 1489–1499.

Stenhammar, J., R. Wittkowski, D. Marenduzzo, and M. E. Cates, 2015, "Activity-Induced Phase Separation and Self-Assembly in Mixtures of Active and Passive Particles," Phys. Rev. Lett. **114**, 018301.

Stramer, B., and R. Mayor, 2017, "Mechanisms and *in vivo* functions of contact inhibition of locomotion," Nat. Rev. Mol. Cell Biol. **18**, 43–55.

Szamel, G., 2014, "Self-propelled particle in an external potential: Existence of an effective temperature," Phys. Rev. E **90**, 012111.

Tailleur, J., and M. E. Cates, 2008, "Statistical Mechanics of Interacting Run-and-Tumble Bacteria," Phys. Rev. Lett. **100**, 218103.

Tailleur, J., and M. E. Cates, 2009, "Sedimentation, trapping, and rectification of dilute bacteria," Europhys. Lett. **86**, 60002.

Tailleur, Julien, Gerhard Gompper, M. Cristina Marchetti, Julia M. Yeomans, and Christophe Salomon, 2022, Eds., *Active Matter and Nonequilibrium Statistical Physics*, Lecture Notes of the Les Houches Summer School Vol. 112 (Oxford University Press, New York).

Takagi, D., J. Palacci, A. B. Braunschweig, M. J. Shelley, and J. Zhang, 2014, "Hydrodynamic capture of microswimmers into sphere-bound orbits," Soft Matter **10**, 1784–1789.

Takaha, Y., and D. Nishiguchi, 2023, "Quasi-two-dimensional bacterial swimming around pillars: Enhanced trapping efficiency and curvature dependence," Phys. Rev. E **107**, 014602.
Takatori, S. C., and J. F. Brady, 2015, "Towards a thermodynamics of active matter," Phys. Rev. E **91**, 032117.
Takatori, S. C., R. De Dier, J. Vermant, and J. F. Brady, 2016, "Acoustic trapping of active matter," Nat. Commun. **7**, 10694.
Takatori, S. C., W. Yan, and J. F. Brady, 2014, "Swim Pressure: Stress Generation in Active Matter," Phys. Rev. Lett. **113**, 028103.
Theurkauff, I., C. Cottin-Bizonne, J. Palacci, C. Ybert, and L. Bocquet, 2012, "Dynamic Clustering in Active Colloidal Suspensions with Chemical Signaling," Phys. Rev. Lett. **108**, 268303.
Thiffeault, J., 2015, "Distribution of particle displacements due to swimming microorganisms," Phys. Rev. E **92**, 023023.
Thompson, A. G., J. Tailleur, M. E. Cates, and R. A. Blythe, 2011, "Lattice models of nonequilibrium bacterial dynamics," J. Stat. Mech. P02029.
Thutupalli, S., R. Seemann, and S. Herminghaus, 2011, "Swarming behavior of simple model squirmers," New J. Phys. **13**, 073021.
Tjhung, E., C. Nardini, and M. E. Cates, 2018, "Cluster Phases and Bubbly Phase Separation in Active Fluids: Reversal of the Ostwald Process," Phys. Rev. X **8**, 031080.
Toner, J., N. Guttenberg, and Y. Tu, 2018a, "Hydrodynamic theory of flocking in the presence of quenched disorder," Phys. Rev. E **98**, 062604.
Toner, J., N. Guttenberg, and Y. Tu, 2018b, "Swarming in the Dirt: Ordered Flocks with Quenched Disorder," Phys. Rev. Lett. **121**, 248002.
Toner, J., Y. Tu, and S. Ramaswamy, 2005, "Hydrodynamics and phases of flocks," Ann. Phys. (N.Y.) **318**, 170–244.
Tsou, A. M., and J. Zhu, 2010, "Quorum sensing negatively regulates hemolysin transcriptionally and posttranslationally in *Vibrio cholerae*," Infect. Immun. **78**, 461–467.
Turci, F., N. B. Wilding, and R. L. Jack, 2024, "Partial and complete wetting of droplets of active Brownian particles," Soft Matter **20**, 2060–2074.
van Beijeren, H., 1982, "Transport properties of stochastic Lorentz models," Rev. Mod. Phys. **54**, 195–234.
van der Linden, M. N., L. C. Alexander, D. G. A. L. Aarts, and O. Dauchot, 2019, "Interrupted Motility Induced Phase Separation in Aligning Active Colloids," Phys. Rev. Lett. **123**, 098001.
Vásárhelyi, G., C. Virágh, G. Somorjai, T. Nepusz, A. E. Eiben, and T. Vicsek, 2018, "Optimized flocking of autonomous drones in confined environments," Sci. Rob. **3**, eaat3536.
Verma, S., and T. Miyashiro, 2013, "Quorum sensing in the squid-*Vibrio* symbiosis," Int. J. Mol. Sci. **14**, 16386–16401.
Vicsek, T., A. Czirók, E. Ben-Jacob, I. Cohen, and O. Shochet, 1995, "Novel Type of Phase Transition in a System of Self-Driven Particles," Phys. Rev. Lett. **75**, 1226–1229.
Weber, S. N., C. A. Weber, and E. Frey, 2016, "Binary Mixtures of Particles with Different Diffusivities Demix," Phys. Rev. Lett. **116**, 058301.
Whitelam, S., K. Klymko, and D. Mandal, 2018, "Phase separation and large deviations of lattice active matter," J. Chem. Phys. **148**, 154902.
Winkler, R. G., A. Wysocki, and G. Gompper, 2015, "Virial pressure in systems of spherical active Brownian particles," Soft Matter **11**, 6680–6691.
Wittkowski, R., J. Stenhammar, and M. E. Cates, 2017, "Nonequilibrium dynamics of mixtures of active and passive colloidal particles," New J. Phys. **19**, 105003.
Wittkowski, R., A. Tiribocchi, J. Stenhammar, R. J. Allen, D. Marenduzzo, and M. E. Cates, 2014, "Scalar ϕ^4 field theory for active-particle phase separation," Nat. Commun. **5**, 4351.
Wittmann, R., C. Maggi, A. Sharma, A. Scacchi, J. M. Brader, and U. Marini Bettolo Marconi, 2017, "Effective equilibrium states in the colored-noise model for active matter I. Pairwise forces in the Fox and unified colored noise approximations," J. Stat. Mech. 113207.
Wittmann, R., U. M. B. Marconi, C. Maggi, and J. M. Brader, 2017, "Effective equilibrium states in the colored-noise model for active matter II. A unified framework for phase equilibria, structure and mechanical properties," J. Stat. Mech. 113208.
Woillez, E., Y. Kafri, and N. S. Gov, 2020, "Active Trap Model," Phys. Rev. Lett. **124**, 118002.
Woillez, E., Y. Kafri, and V. Lecomte, 2020, "Nonlocal stationary probability distributions and escape rates for an active Ornstein-Uhlenbeck particle," J. Stat. Mech. 063204.
Wu, X., and A. Libchaber, 2000, "Particle Diffusion in a Quasi-Two-Dimensional Bacterial Bath," Phys. Rev. Lett. **84**, 3017–3020.
Wysocki, A., J. Elgeti, and G. Gompper, 2015, "Giant adsorption of microswimmers: Duality of shape asymmetry and wall curvature," Phys. Rev. E **91**, 050302.
Wysocki, A., and H. Rieger, 2020, "Capillary Action in Scalar Active Matter," Phys. Rev. Lett. **124**, 048001.
Wysocki, A., R. G. Winkler, and G. Gompper, 2014, "Cooperative motion of active Brownian spheres in three-dimensional dense suspensions," Europhys. Lett. **105**, 48004.
Wysocki, A., R. G. Winkler, and G. Gompper, 2016, "Propagating interfaces in mixtures of active and passive Brownian particles," New J. Phys. **18**, 123030.
Yan, J., M. Han, J. Zhang, C. Xu, E. Luijten, and S. Granick, 2016, "Reconfiguring active particles by electrostatic imbalance," Nat. Mater. **15**, 1095–1099.
Yan, W., and J. F. Brady, 2015, "The force on a boundary in active matter," J. Fluid Mech. **785**, R1.
Yan, W., and J. F. Brady, 2018, "The curved kinetic boundary layer of active matter," Soft Matter **14**, 279–290.
Yang, X., M. L. Manning, and M. C. Marchetti, 2014, "Aggregation and segregation of confined active particles," Soft Matter **10**, 6477–6484.
You, Z., A. Baskaran, and M. C. Marchetti, 2020, "Nonreciprocity as a generic route to traveling states," Proc. Natl. Acad. Sci. U.S.A. **117**, 19767–19772.
Zaeifi Yamchi, M., and A. Naji, 2017, "Effective interactions between inclusions in an active bath," J. Chem. Phys. **147**, 194901.
Zaid, I. M., J. Dunkel, and J. M. Yeomans, 2011, "Lévy fluctuations and mixing in dilute suspensions of algae and bacteria," J. R. Soc. Interface **8**, 1314–1331.
Zakine, R., A. Solon, T. Gingrich, and F. Van Wijland, 2017, "Stochastic stirling engine operating in contact with active baths," Entropy **19**, 193.
Zakine, R., Y. Zhao, M. Knežević, A. Daerr, Y. Kafri, J. Tailleur, and F. van Wijland, 2020, "Surface Tensions between Active Fluids and Solid Interfaces: Bare vs Dressed," Phys. Rev. Lett. **124**, 248003.
Zhang, J., R. Alert, J. Yan, N. S. Wingreen, and S. Granick, 2021, "Active phase separation by turning towards regions of higher density," Nat. Phys. **17**, 961–967.
Zhao, H., A. Košmrlj, and S. S. Datta, 2023, "Chemotactic Motility-Induced Phase Separation," Phys. Rev. Lett. **131**, 118301.
Zhao, Y., R. Zakine, A. Daerr, Y. Kafri, J. Tailleur, and F. van Wijland, 2024, "Active Young-Dupré equation: How self-organized currents stabilize partial wetting," arXiv:2405.20651.